Cerebral Cortex October 2012;22:2375–2391
doi:10.1093/cercor/bhr317
Advance Access publication November 16, 2011

Cell Type–Specific Three-Dimensional Structure of Thalamocortical Circuits in a Column of Rat Vibrissal Cortex

Marcel Oberlaender[1], Christiaan P. J. de Kock[2], Randy M. Bruno[3], Alejandro Ramirez[3], Hanno S. Meyer[1], Vincent J. Dercksen[4], Moritz Helmstaedter[5] and Bert Sakmann[1]

[1]Digital Neuroanatomy, Max Planck Florida Institute, Jupiter, FL 33458-2906, USA, [2]Department of Integrative Neurophysiology, Center for Neurogenomics and Cognitive Research, Neuroscience Campus Amsterdam, VU University Amsterdam, 1081 HV Amsterdam, the Netherlands, [3]Department of Neuroscience, Columbia University, New York, NY 10032, USA, [4]Department of Visualization and Data Analysis, Zuse Institute, D-14195 Berlin, Germany and [5]Department of Biomedical Optics, Max Planck Institute for Medical Research, D-69120 Heidelberg, Germany

Oberlaender and de Kock have contributed equally to this work

Address correspondence to Marcel Oberlaender, Digital Neuroanatomy, Max Planck Florida Institute, 5353 Parkside Drive, MC19-RE, Jupiter, FL 33458-2906, USA. Email: marcel.oberlaender@mpfi.org.

Soma location, dendrite morphology, and synaptic innervation may represent key determinants of functional responses of individual neurons, such as sensory-evoked spiking. Here, we reconstruct the 3D circuits formed by thalamocortical afferents from the lemniscal pathway and excitatory neurons of an anatomically defined cortical column in rat vibrissal cortex. We objectively classify 9 cortical cell types and estimate the number and distribution of their somata, dendrites, and thalamocortical synapses. Somata and dendrites of most cell types intermingle, while thalamocortical connectivity depends strongly upon the cell type and the 3D soma location of the postsynaptic neuron. Correlating dendrite morphology and thalamocortical connectivity to functional responses revealed that the lemniscal afferents can account for some of the cell type- and location-specific subthreshold and spiking responses after passive whisker touch (e.g., in layer 4, but not for other cell types, e.g., in layer 5). Our data provides a quantitative 3D prediction of the cell type–specific lemniscal synaptic wiring diagram and elucidates structure–function relationships of this physiologically relevant pathway at single-cell resolution.

Keywords: barrel cortex, dendrite morphology, in vivo spiking, neural network, VPM innervation

Introduction

Despite a long tradition in neuroscience research to classify neuronal cell types by anatomical parameters, knowledge of relationships between cell type–specific anatomy and functional responses of individual neurons in vivo remains limited. Methods to directly monitor sensory-evoked excitation streams within neuronal circuits, at subcellular and millisecond resolution, are lacking. To overcome these limitations, reverse engineering approaches of reconstructing circuit anatomy and synaptic wiring have been suggested (Markram 2006; Helmstaedter et al. 2007; Wickersham, Finke, et al. 2007; Wickersham, Lyon, et al. 2007). The resulting anatomically realistic models of neural circuits may allow for numerical (in silico) computer simulations (Lang et al. 2011), which will help to unravel circuit functions and their underlying mechanistic principles during sensory-evoked behaviors.

A cortical column is thought to be an elementary functional unit of sensory cortices (Mountcastle 1957; Hubel and Wiesel 1959) and is thus a natural starting point for reconstructing neuronal circuits. In the vibrissal area of rodent somatosensory cortex (S1), a cytoarchitectonic equivalent to a functional column, designated as a barrel column, has been described (Woolsey and Van der Loos 1970). The dimensions of a barrel column are defined by segregated structures (i.e., the barrels) in granular layer 4 (L4). A barrel column primarily processes sensory input from a related principal whisker (PW) on the animal's snout (Welker 1976). Whisker-evoked excitation after touch and presumably during motion (Yu et al. 2006) is mediated by neurons located in the ventral posterior medial (VPM) division of the thalamus. The VPM is part of the lemniscal pathway (Lubke and Feldmeyer 2007) and subdivided into segregated whisker-specific areas, referred to as barreloids (Land et al. 1995). Neurons in a barreloid project predominantly to the corresponding column and delineate its dimensions (Wimmer et al. 2010). To understand how sensory input from a single PW is capable of eliciting simple behaviors, such as gap-crossing (Hutson and Masterton 1986; Celikel and Sakmann 2007), it is essential to quantify the cell type, lemniscal innervation, and, finally, function of the individual neurons of a barrel column.

Here, we report the 3D structure of thalamocortical circuits between VPM and 9 cell types of excitatory neurons of a barrel column in rats. We do so by 1) reconstructing the 3D morphology of individual excitatory somata and dendrites in a barrel column, 2) objectively identifying excitatory cell types, 3) reconstructing the complete 3D morphology of individual VPM axons, 4) registering all morphologies into a standardized reference frame, 5) assembling an anatomically realistic model of a barrel column, and 6) determining the expected cell type–specific and location-specific synaptic innervation by VPM for each excitatory cortical neuron.

Finally, we relate the structure of the reconstructed thalamocortical circuits to previously measured functional data, recorded in vivo after passive whisker deflection (i.e., touch) and during free-whisking (i.e., self-motion of whiskers). This allowed us to investigate how soma location, dendrite morphology, and lemniscal innervation relate to spiking activity during different behavioral states. We find that spontaneous spiking correlates with dendrite length, while whisker-evoked spiking after passive touch correlates with the number of putative VPM synapses for certain cell types.

Materials and Methods

Labeling with Biocytin

All experiments were carried out in accordance with the animal welfare guidelines of the Max Planck Society and Columbia University.

Cortical neurons were filled with biocytin in urethane-anaesthetized or fentanyl-sedated Wistar rats either extracellularly by using juxtasomal recording and electroporation (Pinault 1996) or via whole-cell recording (Margrie et al. 2002). Spiking profiles of these neurons have been previously published (Bruno and Sakmann 2006; de Kock et al. 2007). VPM cells were filled with biocytin by whole-cell recording. Twelve to nineteen hours were subsequently allowed to elapse to permit adequate tracer diffusion. To ensure accurate axonal reconstruction, usually only one VPM neuron was filled per rat. Occasionally, additional VPM neurons were filled but, in these cases, would be targeted 2–3 barreloids away from previous penetrations (a detailed description of whole-cell recordings in VPM can be found in a forthcoming manuscript (M.O., A.R. and R.M.B., unpublished data) Cytochrome C oxidase staining was used to label barrel contours in L4 (Horikawa and Armstrong 1988). The recorded neurons were labeled with the chromogen 3,3′-diaminobenzidine tetrahydrochloride (DAB) (Wong-Riley 1979). Dendrite and VPM axon morphologies were obtained between postnatal days 25 and 170. No obvious differences in innervation patterns were observed at different ages.

Three-Dimensional Reconstruction of Neuron Morphology

Neuron tracings were performed on 50- or 100-μm thick vibratome sections, cut approximately tangential to the D2 barrel column. Ranging from the pia surface to the white matter, 40 or 24 sections were reconstructed per neuron. DAB-stained dendrites were detected manually using Neurolucida software (MicroBrightfield, Williston, VT). Axons were traced using an automated pipeline (Oberlaender et al. 2007; Oberlaender, Broser, et al. 2009). Manual postprocessing of individual sections (Dercksen et al. 2012) and automated alignment of branches across sections (Dercksen et al. 2009), were performed in Amira visualization software (Stalling et al. 2005). Pia and barrel outlines were manually drawn on low resolution images (2×) and added to the tracings in Neurolucida software.

All reconstructed morphologies were transformed into a standardized coordinate system having its origin at the center of the barrel containing the neuron's apical dendrite, or in case of VPM cells, containing the majority of the neuron's axon. The *z*-axis pointed dorsally, parallel to the vertical barrel axis, the *x*-axis laterally toward the center of the first neighboring barrel within the same whisker row (i.e., parallel to the tangential plane).

Average interbouton distances were obtained from high-resolution images stacks (100×, 0.2-μm optical sections). Horizontally projecting axons were chosen for analysis. Interbouton distances were determined by manually marking the 3D location of each bouton along the reconstructed axons. Custom-written routines were used to measure distance along the axons between these markers. Measurements were performed for 1050 boutons from axonal segments in 5 different rats.

Definition of Excitatory Cell Types

Classification of cell types was performed on dendrite reconstructions by using a clustering algorithm (i.e., OPTICS with parameters: minPoints 3, epsilon 6) implemented in WEKA software (http://sourceforge.net/projects/weka/). Cluster analysis was performed with 90 morphological features. Similarity of each feature was analyzed, and features that did not vary within the group of one cell type were neglected. Consequently, the number of features was reduced until a minimal set of features that maintained the initial clustering structure was left. The resultant remaining morphological features to discriminate between cell types are shown in Supplementary Table S1. In awake recording conditions, 30% of the neurons were anatomically identified. Unidentified cells were assigned to cell types based on recording depth (i.e., soma location) and spontaneous spiking. In L4, no subclassifications were assigned.

Assembling an Average Model Column

The tools for assembling average soma–dendrite networks and estimating synaptic connectivity have been described in detail previously (Lang et al. 2011). Here, these tools were applied to reconstruct a 3D model of a cortical barrel column. The reconstruction was based on the average 3D distribution of excitatory neuron somata in the vibrissal cortex, the number and locations of cell types, and the fraction of each cell type in overlap regions.

Briefly, the soma distribution comprised a volume of 550 × 550 × 2000 μm^3. Each soma was assigned to a cell type. 3D dendrite morphologies of respective cell types were inserted, at maximum 50 μm away from their "real" location within the column. Orientation with respect to the vertical column axis (*z*-axis) was preserved. VPM axons were superimposed. Dendrite and axon morphologies were converted into 3D dendrite and axon density distributions, respectively. The resultant distributions were multiplied with spine (0.5 per micron) and bouton (0.33 per micron) densities, respectively. Summing up these neuron-specific distributions resulted in total spine and total bouton distributions. The 3D distribution of potential synaptic contacts for each cortical neuron was then calculated as follows:

$$C_{i,j}(x,y,z) = f(x,y,z) * S_i(x,y,z) * \frac{b_j(x,y,z)}{S(x,y,z)},$$

where $C_{i,j}$ refers to the synapse distribution of neuron i with presynaptic cell type j, S_i to the spine distribution of neuron i, S to the total spine distribution of all neurons in the column, b_j to the bouton distribution of presynaptic cell type j and f denotes a term to correct for missing neuron populations (i.e., inhibitory interneurons). All density distributions were presented with 50-μm voxel resolution. Innervation volumes, 1D, and 2D profiles were derived from these distributions.

Only neurons with their somata located within a cylindrical subvolume (i.e., cross-section: 121 000 μm^2 [Wimmer et al. 2010], height: vertical extents of L2-6) were used for analysis. Neurons outside the cylinder were regarded as septal neurons. The present approach thus accounts for the effect that VPM synapses may be located on dendrites from septal neurons.

All data are given as mean ± standard deviation (SD). Significance level was set 0.05, and statistical analysis was performed in Igor Pro Software.

Results

Reconstruction and Registration of Individual 3D Neuron Morphologies

Figure 1 illustrates the anatomical data used to reconstruct thalamocortical circuits between VPM and excitatory neurons in a cortical barrel column. We reconstructed the 3D dendrite morphology of neurons (n = 95) located in cytoarchitectonic L2-6 and the 3D axon morphology of neurons located in VPM (n = 12). All neurons were filled with biocytin in vivo. Previously, a subset of the cortical neurons were physiologically characterized for spontaneous and whisker-evoked spiking activity after passive touch (de Kock et al. 2007).

We reconstructed the pia surface and respective L4 barrel volumes for each neuron in 3D (Fig. 1*A*). These anatomical landmarks allowed registering all morphologies into a standardized reference system (Fig. 1*B*). This step was essential in that it allowed for comparison of morphologies across animals, while compensating for possible artifacts such as tissue shrinkage or variability in slicing angle of brain sections. Specifically, registration yielded quantitative and comparable morphological parameters, such as the depth of a neuron's soma underneath the pia surface, the total length, 3D span, or the number of branching and ending points of any reconstructed dendrite (Table 1, Supplementary Table S1).

Registering all morphologies into a common reference frame further allowed calculating the structural overlap between VPM axons and cortical dendrites in 3D. This yielded first-order estimates on the number and subcellular innervation pattern of thalamocortical synapses (Fig. 1*C*). Thus, each reconstructed excitatory neuron could be described by the 3D location of its

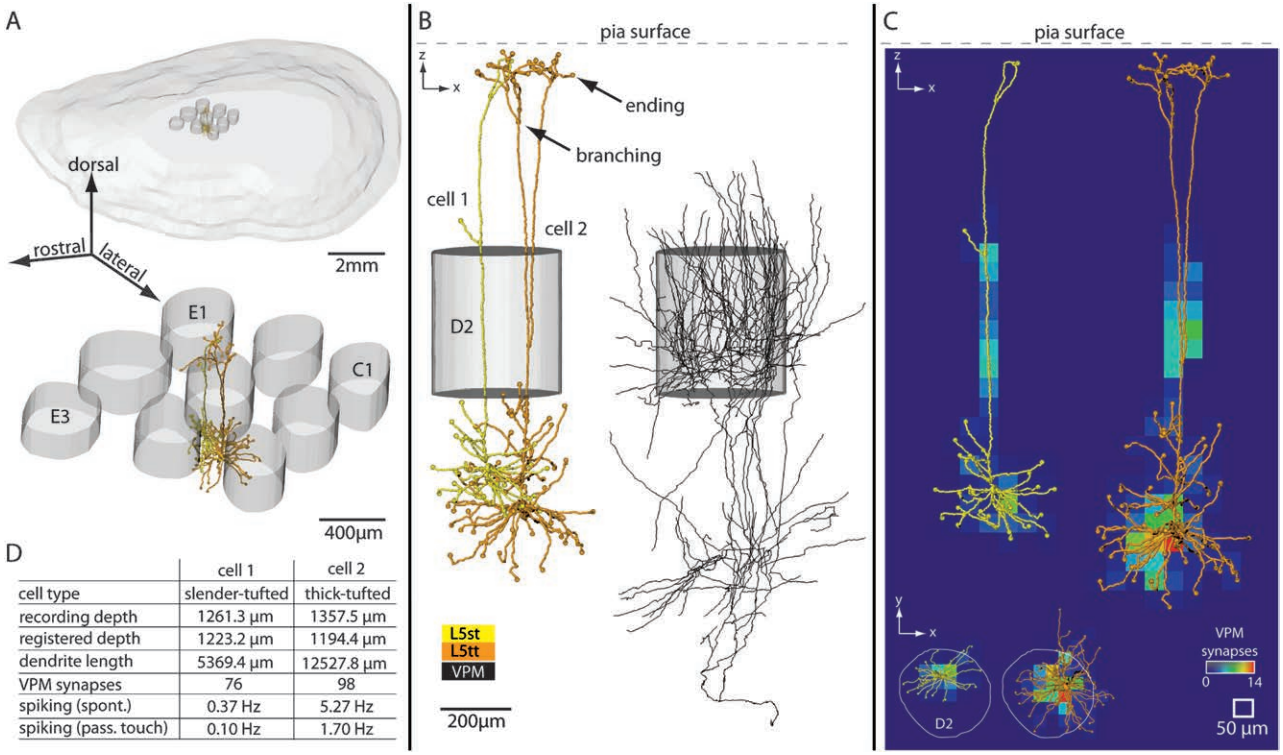

D

	cell 1	cell 2
cell type	slender-tufted	thick-tufted
recording depth	1261.3 µm	1357.5 µm
registered depth	1223.2 µm	1194.4 µm
dendrite length	5369.4 µm	12527.8 µm
VPM synapses	76	98
spiking (spont.)	0.37 Hz	5.27 Hz
spiking (pass. touch)	0.10 Hz	1.70 Hz

Figure 1. Three-dimensional reconstruction and registration of in vivo-labeled dendrite and axon morphologies in a rat barrel column. (*A*) Upper panel: 3D view of pia surface and 9 L4 barrels. Lower panel: Blow up of the 9 barrels. The central barrel contains registered 3D soma–dendrite reconstructions. (*B*) Semicoronal view of registered neurons. Two excitatory neurons of different cell types are located at the same cortical depth (left) and are innervated by thalamocortical axons from VPM (right). (*C*) Structural overlap between registered dendrite and VPM axon morphologies allows determining 3D subcellular innervation of thalamocortical synapses. (*D*) This method of reconstruction and registration allows determining the cell type, anatomical parameters, synaptic innervation, and spiking activity in vivo (spontaneous and evoked by passive whisker touch) for individual neurons. This is illustrated for one example of 2 L5 pyramidal neurons shown in panels *A*–*C*.

Table 1

Cell type–specific morphological parameters of dendrites of excitatory neurons located in a cortical barrel column, obtained from registered 3D reconstructions from in vivo preparations

Cell type	Number of dendrites	Dendrite length (mm)	Basal length (mm)	Apical length (mm)	Dendrite box volume $(mm)^3$	Basal box volume $(mm)^3$	Apical box volume $(mm)^3$	Number of branch points
L2	7.1 ± 1.7	8.58 ± 2.82	4.91 ± 2.20	3.67 ± 1.15	0.049 ± 0.011	0.019 ± 0.011	0.030 ± 0.011	59.7 ± 13.3
L3	5.6 ± 1.8	6.44 ± 0.95	3.53 ± 0.68	2.91 ± 0.71	0.033 ± 0.009	0.014 ± 0.004	0.019 ± 0.007	42.4 ± 10.9
L4py	6.6 ± 0.6	7.49 ± 1.18	4.26 ± 1.04	3.23 ± 0.41	0.049 ± 0.012	0.020 ± 0.009	0.028 ± 0.005	41.0 ± 7.4
L4sp	4.6 ± 2.0	4.23 ± 0.94	2.37 ± 1.61	1.86 ± 0.98	0.026 ± 0.009	0.015 ± 0.013	0.011 ± 0.007	20.0 ± 3.2
L4ss	4.9 ± 1.3	3.38 ± 1.09			0.011 ± 0.005			25.2 ± 15.5
L5st	7.4 ± 1.8	7.71 ± 1.95	4.26 ± 1.31	3.45 ± 0.85	0.102 ± 0.043	0.027 ± 0.011	0.075 ± 0.036	36.9 ± 13.2
L5tt	7.4 ± 1.7	13.84 ± 3.63	5.92 ± 1.86	7.92 ± 1.85	0.264 ± 0.105	0.040 ± 0.020	0.224 ± 0.089	78.5 ± 15.5
L6cc	6.3 ± 0.5	5.86 ± 0.77	3.78 ± 1.11	2.08 ± 0.65	0.056 ± 0.014	0.026 ± 0.009	0.029 ± 0.019	29.4 ± 5.6
L6ct	7.6 ± 1.5	5.90 ± 0.78	2.35 ± 0.38	3.55 ± 0.56	0.035 ± 0.009	0.007 ± 0.001	0.028 ± 0.009	31.6 ± 7.0

soma within the barrel column, unbiased morphological features of its dendrites, spiking activity in vivo, and synaptic innervation by VPM (Fig. 1*D*).

Excitatory Cell Types in a Barrel Column

The morphological features of cortical dendrites were used to subdivide the sample of excitatory neurons into cell types. A density-based cluster algorithm (Ankerst et al. 1999) identified 9 dendritic cell types (Fig. 2) and revealed objective criteria that distinguished between cell types (Supplementary Fig. S1 and, Table S1). The most discriminating differences were observed in the morphology of the apical dendrites and the depth locations of the respective somata within different cortical layers. Cell-type borders were determined by the vertical extents of the cell types (i.e., minimal and maximal registered soma depths) and thus complement cytoarchitectonic definitions of cortical layers (e.g., by soma density [Meyer, Wimmer, Oberlaender, et al. 2010]). These cell type–based boundaries were not sharp and differed from the neuron density–based cytoarchitectonic layer borders. Consequently, somata of different cell types intermingled at the borders between and even within layers (Fig. 2).

L2 pyramids populated the upper part of L2/3 (150–400 µm, minimal and maximal soma depths are presented with ±25 µm resolution, which reflects the precision of registration) and displayed short oblique apical dendrites that spread beyond the tangential column border. In comparison, the L3 pyramids were located in deeper supragranular regions (300–550 µm) and exhibited apical dendrites that projected mostly parallel to the vertical column axis and ended with narrow tufts in L1.

Granular L4 was populated by 3 cell types (Staiger et al. 2004), referred to as L4 pyramids (py), star pyramids (sp), and

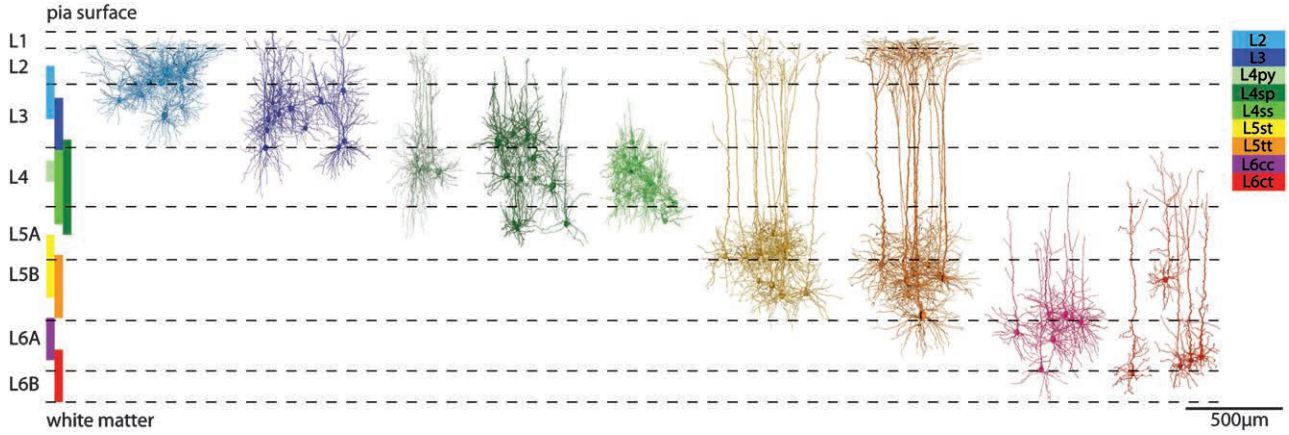

Figure 2. Definition of excitatory cell types in a barrel column. Cluster analysis of morphological features identified 9 excitatory cell types. Registration allowed determining the vertical extent of the cell type–specific soma locations (colored vertical bars). These cell-type borders were not sharp and complement cytoarchitectonic definitions of cortical layers (e.g., using soma density as indicated by the horizontal dashed lines; adopted from Meyer, Wimmer, Oberlaender, et al. (2010). Some of the cell-type borders determined here did not match cytoarchitectonic layer borders (e.g., L4 neurons may be located in cytoarchitectonic layers 3 and 5) and some cell types intermingled within layers (e.g., thick-tufted and slender-tufted neurons in L5).

spiny stellates (ss). Their somata were located at depths between 600 and 700 µm, 500 and 1000 µm, and 550 and 900 µm, respectively. L4py displayed a narrow apical tuft terminating in L1. In contrast, L4sp extended no further than L2 and lacked an apical tuft. The L4ss lacked an apical dendrite altogether.

Infragranular L5 contained 2 types of pyramidal neurons, slender (st)- and thick-tufted (tt) pyramids (Wise and Jones 1977). The apical tuft dendrites of L5tt pyramids extended beyond the tangential column borders, while those of L5st pyramids did not. The somata of these 2 types intermingled (1000–1300 µm and 1100–1400 µm), apart from ~100-µm thick regions directly underneath L4 and above L6, which were exclusively populated by L5st and L5tt pyramids, respectively.

Finally, the clustering identified 2 types of excitatory neurons in L6. The 2 cell types differed in their soma locations and dendrite morphology. Neurons of the first cell type were located at depths between 1400 and 1600 µm and displayed a short apical dendrite that lacked a tuft and terminated at the border between L4 and 5. In contrast, neurons of the second cell type extended apical dendrites into L4 that displayed narrow tufts. In our sample, they were located deeper within L6 at depths between 1550 and 1800 µm (with the exception of one cell that was located within L5 [~1200-µm depth] but otherwise showed the characteristic morphological features of this cell type). The dendrite morphologies of the 2 cell types resembled those of neurons which have previously been classified by characteristic axon projection patterns into L6 corticocortical (cc) and corticothalmic (ct) pyramids (Kumar and Ohana 2008). This naming convention was thus adopted for the present study.

Cell Type–Specific 3D Distribution of Excitatory Somata in a Barrel Column

To quantify the number of excitatory neurons per cell type in a barrel column, we stained slices with NeuN to specifically visualize the location of all neuron somata (Meyer, Wimmer, Oberlaender, et al. 2010). Using 3D confocal microscopy and automated soma detection software (Oberlaender, Dercksen, et al. 2009), we obtained the number and 3D distribution of all neuron somata within 9 barrel columns and their surrounding septa (Supplementary Fig. S2). The average distribution of inhibitory neurons in a cortical barrel column (Meyer et al. 2011) was subtracted from the distribution of all neurons. The resultant average 3D distribution of excitatory somata was combined with the above described vertical cell-type borders (and overlaps) and previously reported dimensions of a cortical barrel column (i.e., cylinder with 121 000 µm^2 cross-sectional area [Wimmer et al. 2010]). This combination allowed subdividing the average excitatory soma distribution into 9 soma domains, which yielded the number and 3D locations of excitatory somata for each cell type (Fig. 3*A*, Table 2). The cylindrical shaped model column contained ~15 000 excitatory somata in total and was referred to as the "soma column" (Fig. 3*B*).

Cell Type–Specific 3D Distribution of Excitatory Dendrites in a Barrel Column

Next, somata were replaced by 3D soma–dendrite morphologies of the corresponding cell types (Fig. 3*C*). Reconstructed morphologies were reregistered to their new location, and orientation with respect to the vertical column axis was preserved. Thus, even though the sample of reconstructed dendrite morphologies was limited for each cell type, the assembling process (Lang et al. 2011) guaranteed that dendrite morphologies at any location in the model column (in silico) resembled those that would be found at approximately the same locations in a real column (in vivo).

The distribution of spines along the dendrites may be location specific and cell-type specific (Romand et al. 2011). However, as a first-order estimate, we assumed a constant and uniform distribution of spines (i.e., 0.5 spines per 1-µm dendrite) for each cell type (Larkman and Mason 1990) and converted the 3D dendrite distribution into a 3D spine distribution (Fig. 3*D*). While the soma distribution displayed pronounced density peaks in cytoarchitectonic L4 and L6 (Fig. 3*B*), the spine distribution was more homogeneous along the vertical column axis, reaching maximal densities in the center of L4 (i.e., the barrel) and at the border between L1 and L2. The latter reflected high densities of apical tufts from dendrites of multiple cell types (i.e., L2, L3, L4py, L5st, L5tt).

Calculating the minimal volume (i.e., 3D envelope) that comprised all dendrites–spines (Fig. 3*C*), we were able to determine the 3D dendrite–spine innervation domain from all excitatory neurons located in the soma column and thus referred to this volume as the "dendrite column." Its tangential extent exceeded the dimensions of the soma column, with dendrites reaching into septa between columns and even to surrounding columns.

Furthermore, we determined the dendrite–spine innervation domains for each of the 9 cell types individually (Fig. 4*A*). This allowed calculating mutual overlaps between cell types with higher precision, when compared with the overlap of their somata (Supplementary Fig. S3 and Table S2). All cell types displayed dendrite–spine domains that overlapped to different degrees. No cell type occupied an area of the column exclusively. However, some extreme cases emerged. On the one hand, we found cell types that shared their entire dendrite–spine volume with another cell type. This was the case for L2 pyramids, ~95% of whose dendrites were contained within the apical tuft volume of L5tt pyramids. On the other hand, some cell types did not share dendrite–spine domains with other cell types at all. For example, dendrites from L6cc cells share almost no volume with cells in the granular and supragranular layers. Another example was the dendrite domain of L4ss cells, which was well separated from the dendrite innervation of L2 neurons.

In addition, we quantified the 3D spine density distribution within the respective dendrite innervation volumes (Fig. 4*A* and Table 2). All dendrite–spine innervation domains extended beyond the tangential borders of the soma column, which was particularly pronounced for L2 and L5tt pyramids (Supplementary Fig. S4), with 9.2% and 11.2% of their spines being located within adjacent septal regions, respectively (Table 2). Furthermore, collapsing the density distribution to 1D profiles along the vertical axis (Fig. 4*B*) allowed for direct comparison with previously reported profiles obtained from dendrite morphologies traced from in vitro preparations (Meyer, Wimmer, Hemberger, et al. 2010).

Excitatory Cell Types in VPM

In order to relate the 3D networks of excitatory somata and dendrites to thalamocortical innervation by VPM, we quantified the intracortical 3D patterns of individually reconstructed VPM axon arbors. The length of individual VPM axons within the vibrissal area ranged from 32.47 to 72.39 mm (mean: 54.05 ± 12.91 mm). All VPM axons delineated the tangential borders of a barrel column and displayed 2 major innervation zones, one in L4 and a second at the border between L5 and L6, on average at cortical depths of ~750 μm and 1350–1400 μm underneath the pia, respectively. The 2 density peaks were usually separated by a density minimum located in the upper part of L5, at ~1100-μm depth. In our sample, VPM innervation did not extend beyond the border of L2 and L3, at ~300-μm depths.

Even though the general VPM innervation pattern was stereotypic, individual VPM axons differed in their total length, the ratio between the L4 and L5/6 peaks and in particular, in their 3D subcellular structure. Based on the latter, we assigned 4 VPM cell types: 1) core, 2) subbarrel/core, 3) core/tail, and 4) head neurons (Fig. 5). The naming convention was adopted from previous studies (Pierret et al. 2000; Furuta et al. 2009), which related VPM projection patterns to soma locations within the barreloid. The part of the barreloid closest to the VPM/Po (i.e., posterior thalamic nucleus) border was named head, the central part core and the most distal part from the VPM/Po border was named tail. Subbarrel/core axons innervated only around ~30–50% of the barrel volume in L4 and may give rise to subbarrels, whose existence was suggested previously (Land and Erickson 2005; Furuta et al. 2011). In contrast, core and core/tail cells displayed more homogeneous innervation of the entire barrel, reaching the highest density in the barrel center. Core/tail neurons displayed additional sparse innervation of surrounding septa and columns, particularly in infragranular layers. Head neurons delineated the tangential barrel borders and extended into adjacent septal regions in L4. However, due to the limited number of reconstructed morphologies per cell type, this classification was neglected for the subsequent estimates of thalamocortical connectivity.

Cell Type–Specific 3D Distribution of VPM Axons in a Barrel Column

Previous reports estimated the number of neurons per barreloid to be 250–300 (Land et al. 1995). We confirmed this number to be 285 ± 13, using automated analysis of NeuN-labeled sections in rat thalamus (Oberlaender 2009). Assuming that the reconstructed VPM morphologies reflected the variability of thalamocortical axons within the vibrissal cortex, we extrapolated the 12 reconstructions to one barreloid (i.e., to 285 VPM neurons). First, we superimposed the 12 registered axon arbors and converted them into a 3D axon density distribution with 50-μm voxel resolution. Then, we scaled up to 285 axons by multiplying each voxel with 23.5, which yielded approximately the 3D distribution of thalamocortical axons from a single barreloid within the vibrissal cortex (Fig. 3*E*). Finally, to relate this distribution to innervation densities that may allow estimates of synaptic connectivity, we determined the distance between boutons ($n = 1050$) along the VPM axons. We found swellings that were likely to correspond to "en passant," and in some cases, "terminaux" boutons (De Paola et al. 2006) along all axon branches and in all regions. The interbouton distance was 3.43 ± 0.13 μm and, more importantly, independent of the axon's location and animal ($n = 5$). Thus, we converted the VPM axon distribution into a 3D VPM bouton distribution (Fig. 3*F*).

The tangential dimensions of this "VPM innervation column" exceeded the tangential borders of the average soma column. Only ~57% of the total number of axon-boutons was located within the soma column volume. In particular, the infragranular projections displayed most axon-boutons in septal regions (~43% in column), while ~2/3 of the granular and supragranular projections were located in the soma column volume (Supplementary Fig. S5). However, the tangential extent of the dendrite column was wider when compared with the soma column, in particular in infragranular layers. Thus, the dendrite column comprised most of the ~5 130 000 VPM boutons from a single barreloid (Fig. 3*E*).

Cell Type– and Location-Specific Thalamocortical Connectivity in a Barrel Column

In the neocortex, synapses of excitatory neurons are associated with en passant or terminaux boutons (De Paola et al. 2006). Thus, for the present study, axonal length and bouton measurements were regarded as predictive of thalamocortical connectivity (Peters 1979). Using a recently reported tool

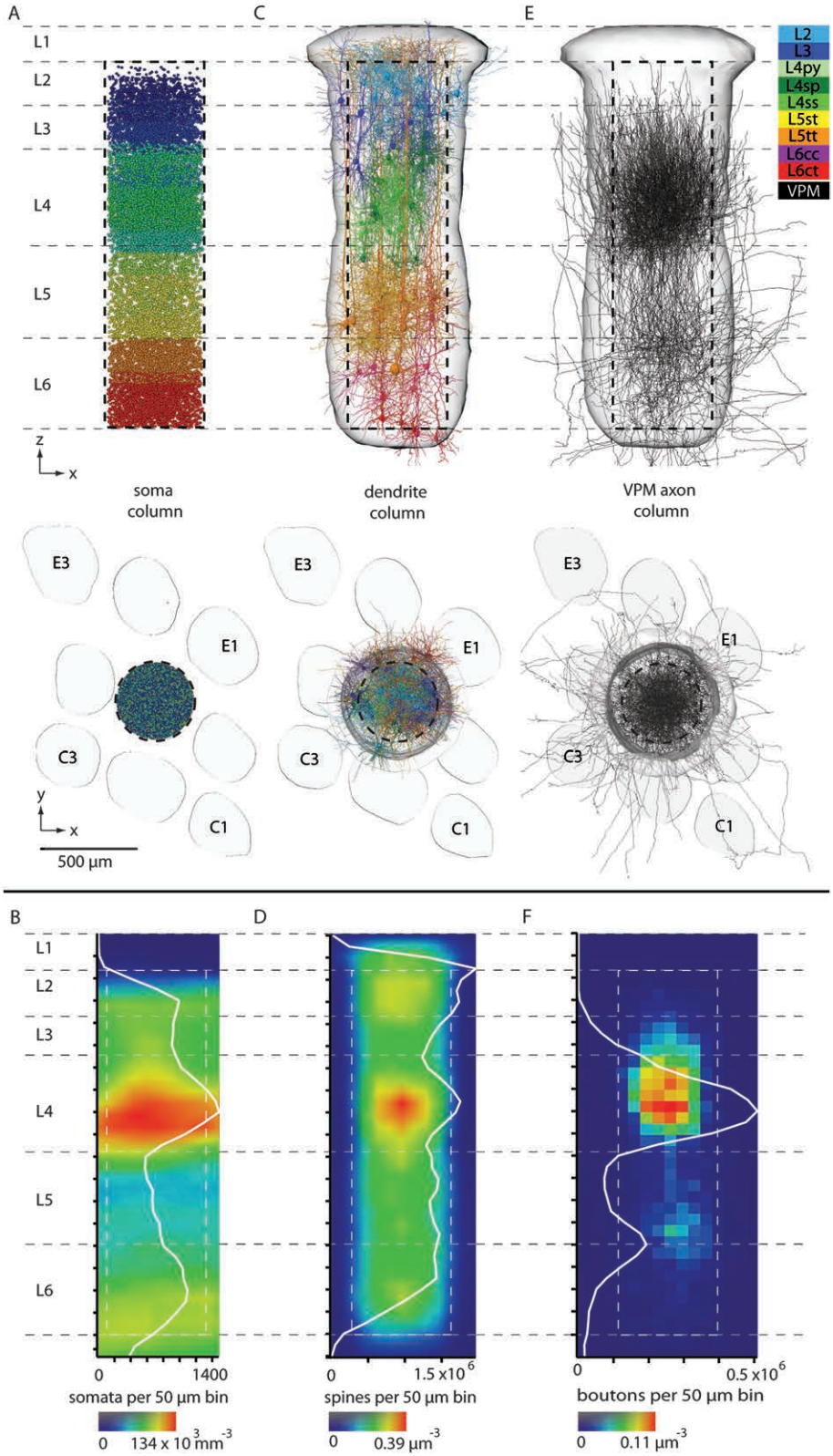

Figure 3. Three-dimensional reconstruction of thalamocortical circuits between VPM and excitatory neurons in a barrel column. (*A*) Semicoronal (upper panel) and tangential (lower panel) view of the 3D cell type–specific network of excitatory neuron somata in a barrel column (dashed box: dimensions of the soma column). Three-dimensional soma locations of various cell types intermingle within cytoarchitectonic layers (note that neurons in L1 are not shown). (*B*) The 3D density distribution of all excitatory neuron somata is superimposed with the 1D density profile along the vertical column axis. (*C*) 3D cell type–specific network of dendrites of excitatory neurons. The gray volume refers to the 3D envelop surrounding the dendrites from all neurons located within the soma column (i.e., dendrite column). (*D*) The dendrite network is converted into a 3D spine distribution, which is also shown as the 1D spine density profile along the vertical column axis. (*E*) Superposition of individual intracortical 3D patterns of VPM axons ($n = 12$) in semicoronal and tangential view. (*F*) The VPM axon network is extrapolated to one barreloid and converted into a 3D bouton distribution, which is also shown as a 1D profile along the vertical column axis. Dashed horizontal lines represent cell type–derived layer borders as shown in Fig. 1.

Table 2
Estimated cell type–specific morphological parameters of 9 ensembles of excitatory neurons in an average barrel column

Cell type	Average depth (μm)	Number of cells (per column)	Number of spines (per cell)	Number of spines (per type and column %)	Number of VPM synapses (per cell)	Number of VPM synapses (per type and column %)
L2	268 ±74	1095 ± 21	4016 ± 1218	4 301 092, 90.8	6 ± 12	7237, 98.0
L3	438 ± 98	1605 ± 18	3178 ± 479	5 049 237, 94.2	66 ± 63	92 762, 97.6
L4py	647 ± 40	459 ± 18	3387 ± 984	1 598 495, 95.3	341 ± 166	149 289, 98.1
L4sp	678 ± 168	2570 ± 17	2474 ± 849	6 331 121, 94.8	278 ± 159	712 968, 98.2
L4ss	733 ± 98	2752 ± 46	1709 ± 490	4 782 075, 96.7	246 ± 123	697 065, 98.8
L5st	1137 ± 101	999 ± 25	3951 ± 1044	3 943 459, 91.4	165 ± 86	157 432, 96.7
L5tt	1208 ± 86	1613 ± 20	6561 ± 1618	10 615 922, 88.8	195 ± 82	318 295, 95.4
L6cc	1431 ± 145	1661 ± 16	3074 ± 373	5 167 944, 92.9	131 ± 52	225 724, 95.9
L6ct	1526 ± 242	2226 ± 9	2942 ± 395	6 522 316, 95.3	139 ± 84	311 955, 97.5
Total		14 981 ± 55		48 311 659		2 672 727

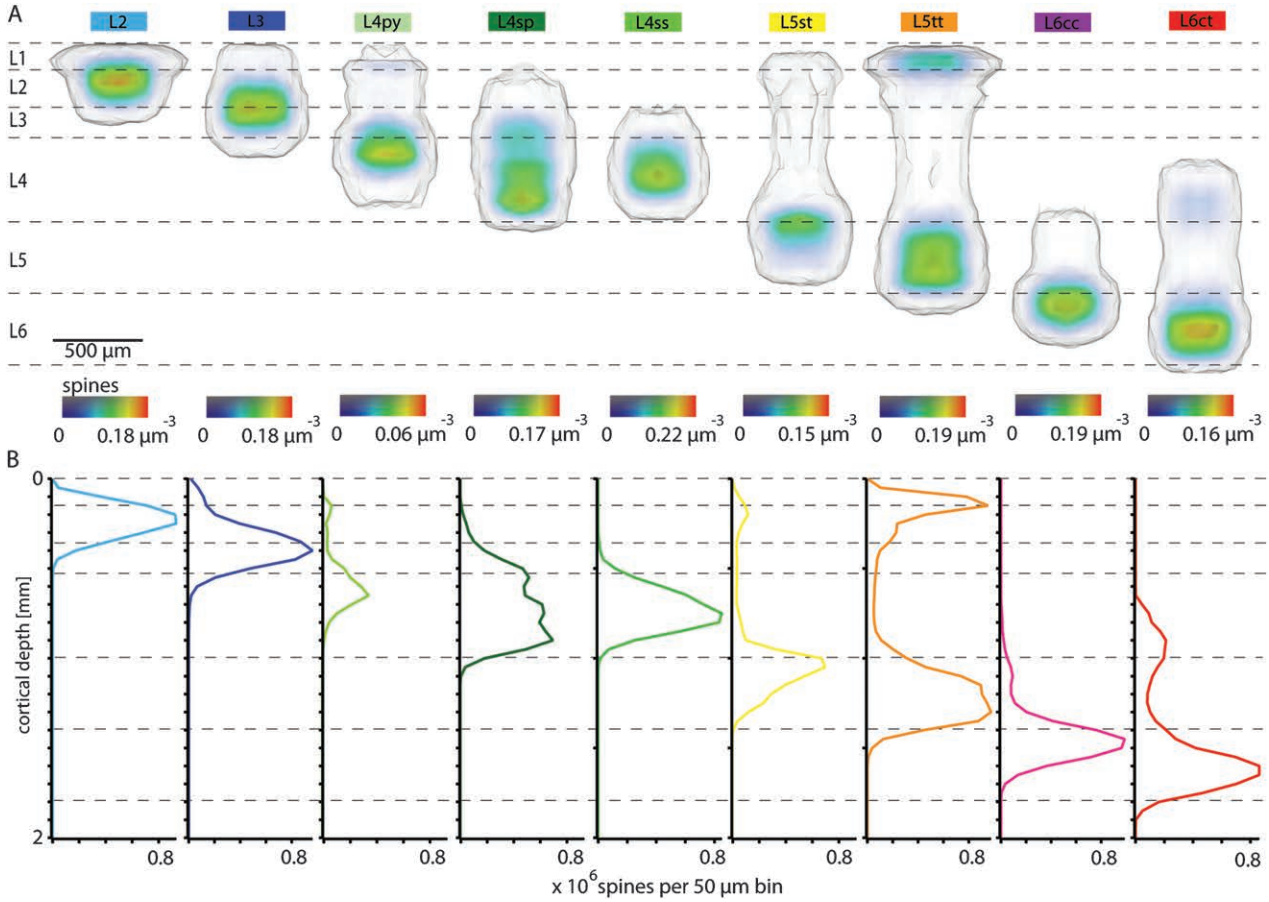

Figure 4. Cell type–specific 3D dendrite–spine distributions within a barrel column. (*A*) Semicoronal view of cell type–specific 3D dendrite–spine densities and innervation volumes for the 9 excitatory cell types. (*B*) Cell type–specific 1D spine density profiles along the vertical column axis.

(Lang et al. 2011), we superimposed the excitatory dendrite column (i.e., 3D cell type–specific spine distributions of ~15 000 neurons) with the VPM innervation column (i.e., 3D bouton distribution of 285 VPM axons). By calculating the structural overlap between the cortical and the VPM neurons, we obtained a first-order estimate of the number and 3D distribution of putative synaptic contacts from a single barreloid with each neuron in the model column (Table 2). L4py neurons received on average the most synaptic contacts per cell (341 ± 166), followed by L4sp (278 ± 159), L4ss (246 ± 123), L5tt (195 ± 82), L5st (165 ± 86), L6ct (139 ± 84), L6cc (131 ± 52), L3 (65 ± 63), and L2 (7 ± 12).

As for the cell type–specific spine distributions, we calculated the 3D volume around the respective synapse distributions (Fig. 6*A*) and collapsed the densities to 1D synapse profiles along the vertical axis (Fig. 6*B*). The VPM synapse distributions displayed in general only a single innervation peak. However, 2 exceptions were found. First, L6ct neurons showed 2 VPM innervation domains, the smaller one in their basal dendrites in L6 and the major one in their apical tuft dendrites in L4. Second, a similar pattern was observed for L5tt neurons, where the VPM innervation peaked within the lower basal dendrites in L5, but a second, less pronounced, peak existed in the apical oblique dendrites in L4. Interestingly, cell types located within the same layer, that is, the 3 cell types in L4 or L5st and L5tt neurons, displayed very different VPM innervation patterns. In particular, L5st neurons had the

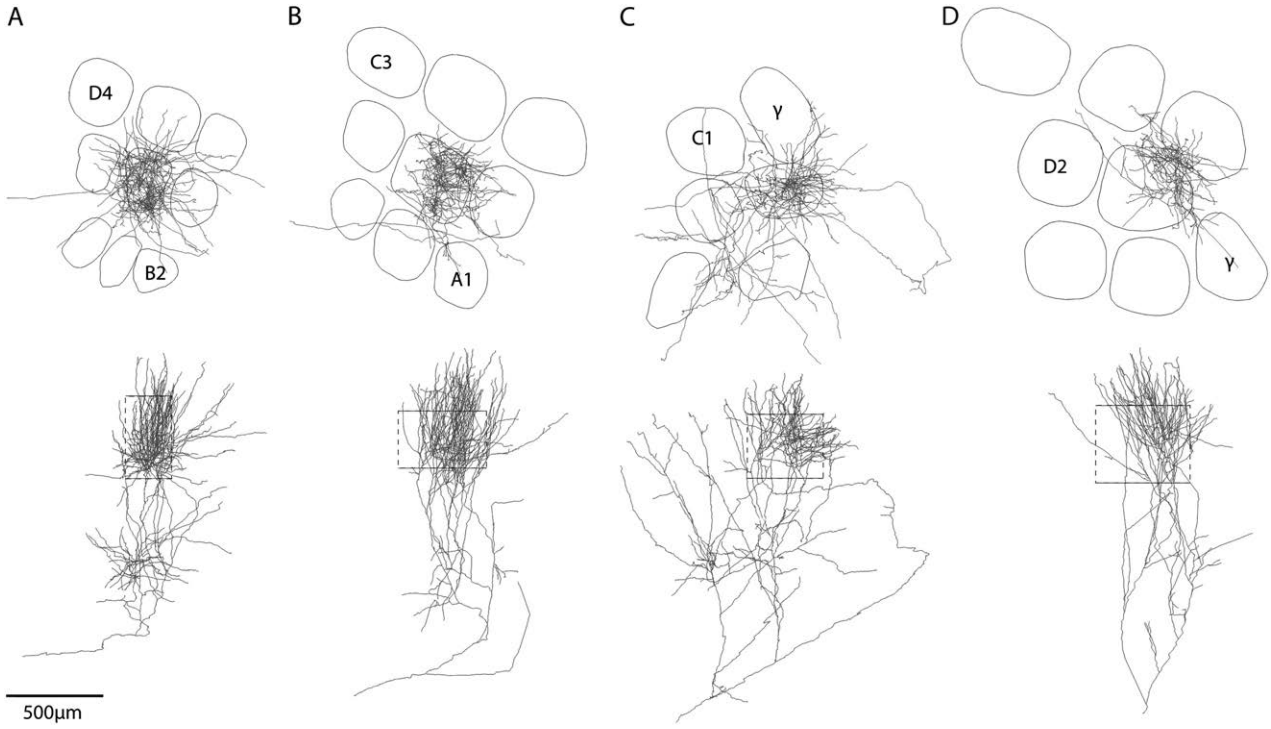

Figure 5. Three-dimensional reconstructions of individual thalamocortical axons in a barrel column. Examples of complete intracortical 3D axon projection patterns of individual VPM neurons. Based on differences in subcellular 3D innervation patterns, we classified 4 different neuron types in a VPM barreloid. (*A*) VPM-core. (*B*) VPM-subbarrel core. (*C*) VPM-core/tail. (*D*) VPM-head. The naming convention was adopted from previous reports that related the projection pattern to the soma location within the barreloid (see Results).

highest innervation density within their apical oblique dendrites in L4, while L5tt received most synapses in their lower basal dendrites in L5 and L6.

In addition to the average number of potential VPM synapses per cell, the present approach of reconstructing the 3D circuit structure at subcellular resolution allowed investigating the influence of dendrite morphology and soma location on thalamocortical connectivity. The relatively large SDs of the average number of VPM synapses per cell were only partly reflected by the differences in dendrite length, which usually varied no more than about 20% within the sample of a respective cell type (Table 1). Thus, the soma location of a cell had to be a major determinant of the number of VPM synapses.

We found substantial differences in the estimated synapse numbers and subcellular distributions for different soma locations along the vertical and tangential column axes (Fig. 7). While some cell types showed rather invariant numbers of potential synaptic contacts with respect to the vertical soma location, L3, L4ss, L4sp, and L5st cells displayed strong variations (Fig. 7*A–C*). For example, as VPM afferents respect the border between L2 and L3, L3 pyramids close to L2 received fewer synapses (22 ± 14) when compared with L3 neurons close to L4 (140 ± 61). Furthermore, VPM innervation was restricted to the lower basal dendrites of L3 cells close to L2, while L3 pyramids close to L4 displayed more homogeneous innervation of basal and apical oblique dendrites (Fig. 7*A*). Consequently, the average subcellular VPM innervation pattern of L3 pyramids displayed most synapses within the lower part of the basal dendrites (Fig. 7*B*). Similar depth dependencies were found for L4ss and L4sp neurons. If located close to L3, L4ss and L4sp neurons received fewer synaptic contacts (172 ± 64 and 115 ± 52, respectively) when compared with cells close to the L5 border (276 ± 154 and 241 ± 98, respectively). Another example were L5st neurons that had most VPM synapses when their somata were close to L4 (218 ± 91), while cells deeper within L5 displayed less synapses (119 ± 45).

In addition to vertical dependencies, the number of potential VPM synapses per neuron decreased, similarly for all cell types, with increasing distance between the soma and the barrel column center (BCC, Fig. 7*D–F*). For example, the L4ss neuron shown in Figure 7*D* (left panel) was located at the BCC, had 503 VPM synapses and displayed an almost symmetric dendrite and thus VPM innervation pattern. In contrast, the L4ss cell shown in Figure 7*D* (right panel) was located at the column border, had only 235 VPM synapses and displayed a polarized dendrite morphology pointing toward the BCC.

Thus, location-depended differences in dendrite morphology, in combination with location-depended differences in VPM bouton density, critically influenced the total number and subcellular innervation patterns of individual neurons, even if they were of the same cell type. In consequence, innervation patterns averaged across all neurons of a particular cell type (e.g., L3, Fig. 7*B* or L4ss, Fig. 7*E*) may conceal differences between individual neurons.

Relationships between 3D Structure and In Vivo Responses of Thalamocortical Circuits in a Barrel Column

A subset of the morphologically reconstructed cortical neurons were physiologically characterized in the anesthetized rat previously (de Kock et al. 2007). This allowed determining the

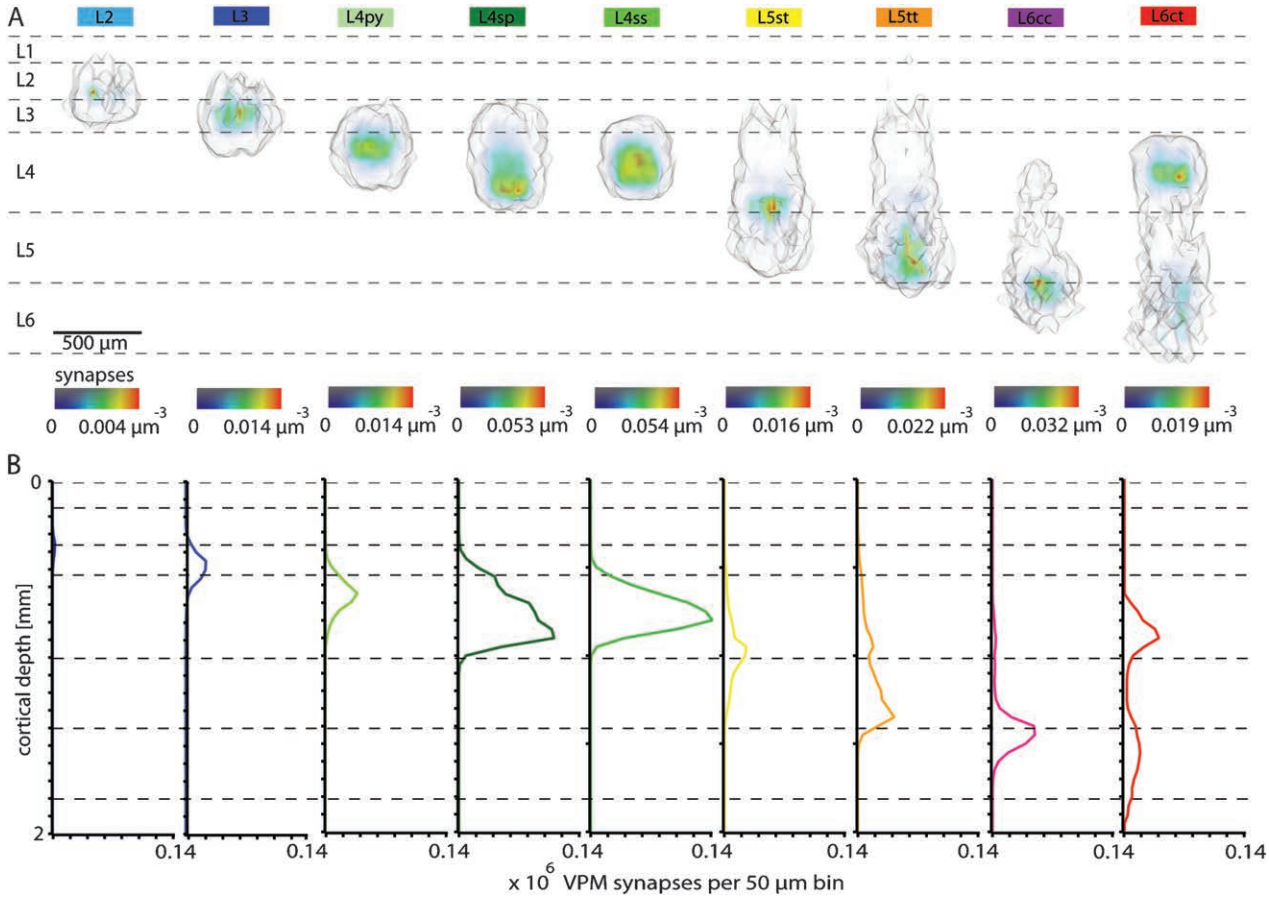

Figure 6. Cell type–specific 3D VPM synapse distributions within a barrel column. (*A*) Semicoronal view of 3D cell type–specific synapse distributions determined by structural overlap between ~15 000 excitatory dendrites and 285 VPM axons. (*B*) Cell type–specific 1D VPM synapse profiles along the vertical column axis. L5tt and L6ct pyramids show bimodal profiles of VPM synapses.

cell type–specific spontaneous and whisker-evoked spiking rates after passive whisker touch for each individual cell. Since the somata of different cell types intermingled within and across cortical layers, the present approach allowed for a more precise assessment of spiking activity, when compared with previous reports of layer-specific spiking responses (Fig. 8, Table 3). Thus, we were able to establish cell type–specific correlations between the spiking activity in vivo of each individual cell and 3D structural parameters, such as its dendrite length or number of thalamocortical synapses (Fig. 9).

As spiking activity of individual neurons is determined by a variety of subcellular, cellular, and networks properties, correlations between spiking and structural parameters were expected to be low. However, we found several significant correlations between cell type–specific spiking and anatomical quantities. We determined the correlation between spontaneous spiking frequencies in the anesthetized state and total dendrite length of each cell. The correlation coefficient was remarkably high (Pearson correlation coefficient $r = 0.76$, $P < 0.0001$, Fig. 9*A*).

Furthermore, we determined the correlation between the estimated number of putative VPM synapses of each neuron and its whisker-evoked spiking, 0–20 ms and 0–50 ms after passive touch, respectively. For both time windows, correlation coefficients were similar. Thus, we show the results only for the 0- to 50-ms time window, where the correlation between evoked spiking and VPM synapses was at trend level ($r = 0.22$, $P = 0.11$, Fig. 9*B*). Interestingly, for multiple cells, the evoked spiking seemed to correlate well above trend level with the respective number of VPM synapses. We thus performed the correlation analysis for each cell type individually. This revealed that the correlation between evoked spiking after passive touch and the number of putative VPM contacts was significantly high for L3 ($r = 0.79$, $P = 0.11$ at trend level), L4ss ($r = 0.92$, $P = 0.03$) and L6cc neurons ($r = 0.89$, $P = 0.04$). The remaining cell types displayed no or only weak correlations, for example, L5st ($r = 0.22$, $P = 0.49$) and L5tt ($r = -0.22$, $P = 0.57$) neurons (Fig. 9*C*).

Furthermore, we reported a similar data set for spiking during quiet and free-whisking periods in the awake rat (de Kock and Sakmann 2009). This enabled us to investigate structure–function relationships across different behavioral states. First, we determined the correlations between the average cell type–specific spontaneous spiking and average dendrite length during anesthetized and awake conditions. Since cell type–specific spontaneous spiking in the anesthetized and awake state were similar, correlations for both states were high ($r = 0.85$ and $r = 0.80$, $P = 0.004$ and $P = 0.01$, Fig. 9*D*). Finally, we determined the correlation between the average whisker-evoked spiking after passive touch and spiking during whisker motion, respectively, with the average number of putative VPM synapses of each cell type. As expected from the

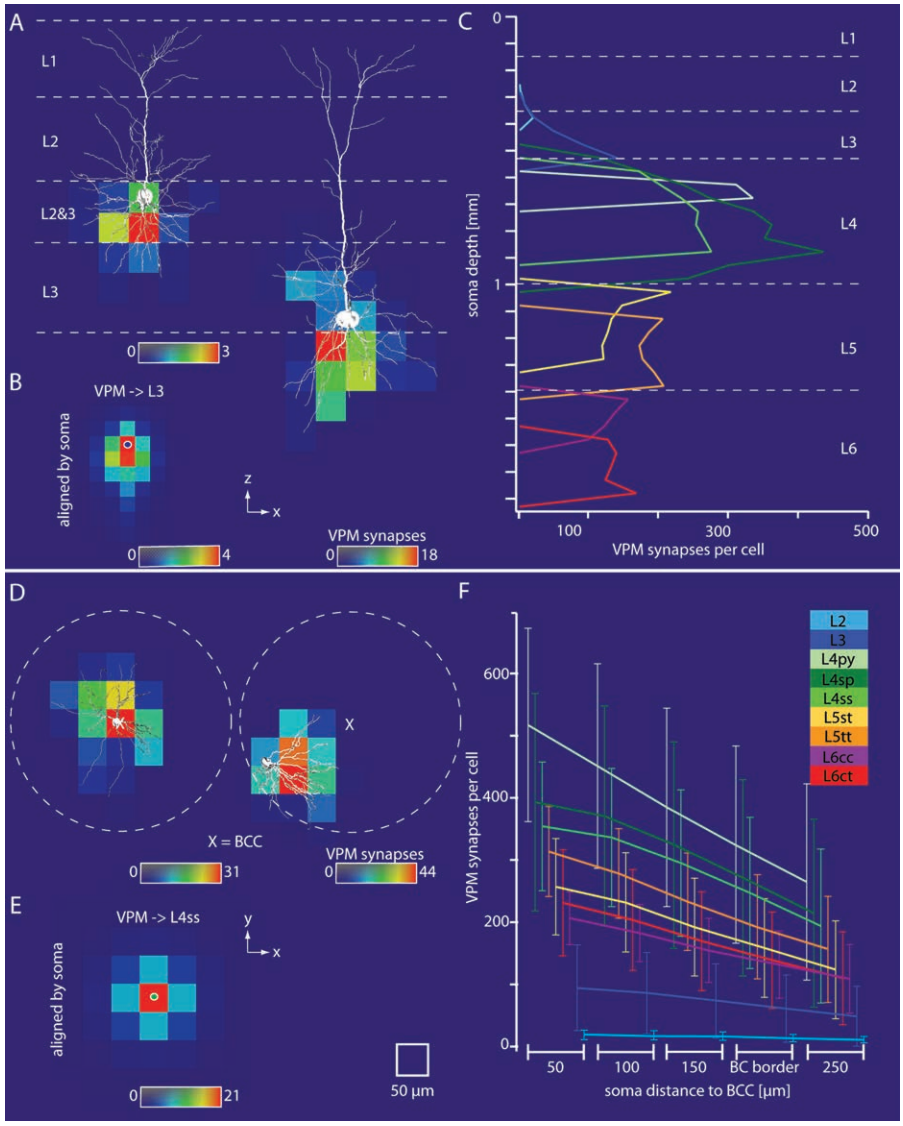

Figure 7. The number and subcellular distribution of VPM synapses is cell type– and location-specific. (*A*) VPM innervation respects the border between L2 and L3 resulting in location-specific numbers and innervation patterns of L3 neurons along the vertical column axis. L3 pyramids close to L2 have synaptic contacts mostly within their lower basal dendrites, while L3 pyramids display more homogeneous innervation patterns of the basal and apical oblique dendrites. (*B*) Averaging across all L3 neurons (aligned by their somata) results in an innervation pattern that is asymmetric, suggesting that all L3 neurons receive VPM input within their lower basal dendrites. (*C*) For most cell types, the number of synaptic VPM contacts per neuron depends on its soma location along the vertical column axis. (*D*) The number of synaptic contacts between VPM and excitatory neurons in L4 decreases with increasing distance between the soma and the BCC. L4ss neurons at the BCC display symmetric dendrite patterns. L4ss cells at the column border have polarized dendrites pointing toward the barrel center. In combination with higher VPM innervation at the BCC, the number and innervation patterns of VPM synapses are location specific along the tangential column axis. (*E*) Averaging across all L4ss neurons results in a radial symmetric innervation pattern, which conceals location-specific profiles. (*F*) The number of VPM synapses per neuron decreases with the distance from the soma to the BCC for all cell types. Neurons were binned in radial rings of 50,100,150,196.3 (BC border) and 250-µm radius centered on the BCC.

analysis at single cell level, the correlation coefficient for passive touch was high ($r = 0.68$, $P = 0.04$), but we did not find a significant correlation between the number of VPM synapses and spiking activity during whisker motion ($r = 0.54$, $P = 0.21$, Fig. 9*E*).

In conclusion, the dendrite length of individual cortical neurons, obtained by 3D reconstruction and registration of in vivo labeled neurons, predicts spontaneous spiking activity of these cells in both anesthetized and awake conditions. Furthermore, structural overlap between VPM axons and cortical dendrites predicts spiking activity after passive whisker touch for individual L3, L4ss, and L6cc neurons. In contrast, evoked spiking of the remaining cell types as well as spiking during whisker motion cannot be predicted by dendrite length or VPM innervation alone.

Discussion

Three major assumptions in reconstructing the thalamocortical circuits between VPM and excitatory neurons within an anatomically realistic model of a barrel column must be assessed critically. First, we extrapolated the limited set of morphologies to ensembles. Secondly, we classified cell types by soma location and dendrite morphology, and finally, the

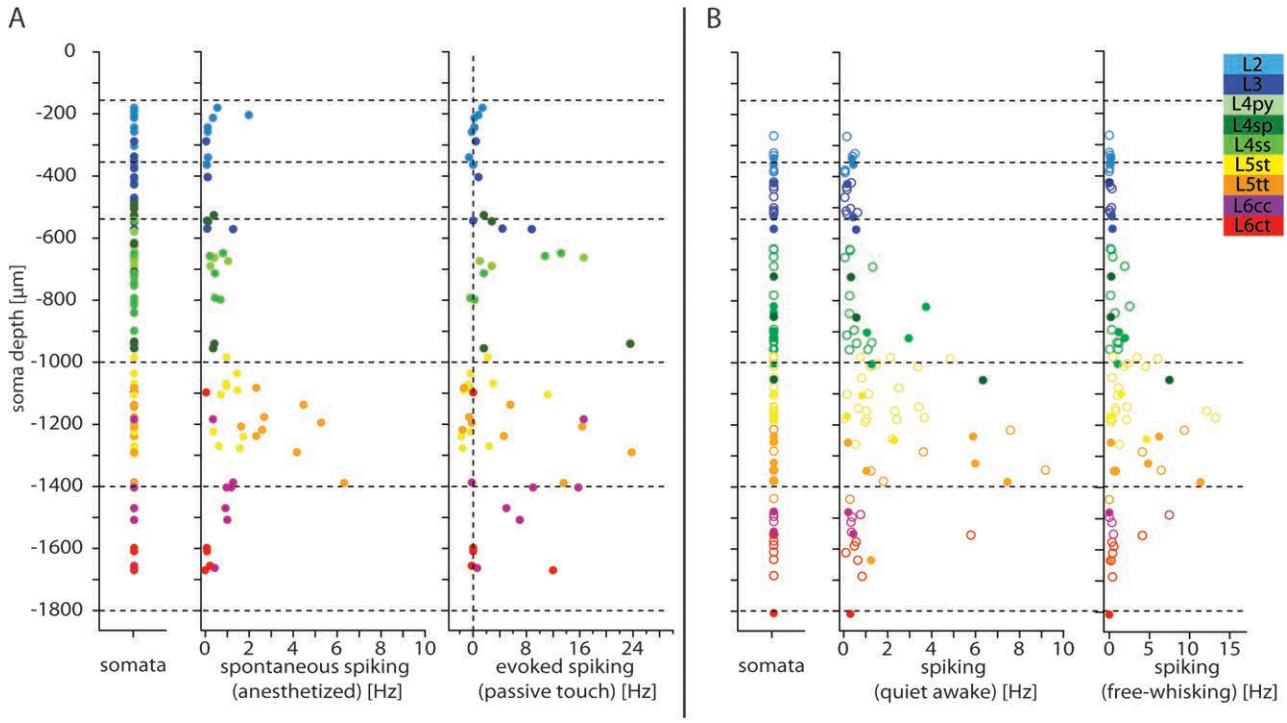

Figure 8. Cell type–specific spiking of individual neurons during different behavioral states. (*A*) Left panel: Vertical locations of all reconstructed somata. Center panel: spontaneous spiking in the anesthetized state. Right panel: evoked spiking (i.e., difference to spontaneous activity), 0–50 ms after passive touch. (*B*) Left panel: Vertical locations of somata (closed circles mark anatomically identified cells; open circles mark cells assigned by depth and spontaneous spiking). Center panel: Spontaneous spiking activity in awake state. Right panel: Spiking activity during free whisking.

Table 3
Cell type–specific spiking activity of excitatory neurons in a cortical barrel column under anesthesia and in awake conditions

Cell type	Spontaneous spiking anesthetized (Hz)	Evoked spiking passive touch (Hz)	Cell type	Spontaneous spiking awake (Hz)	Spiking free whisking (Hz)
L2	0.47 ± 0.69	0.26 ± 0.66	L2	0.23 ± 0.19	0.06 ± 0.07
L3	0.32 ± 0.53	2.88 ± 3.75	L3	0.25 ± 0.20	0.16 ± 0.16
L4py	0.56 ± 0.42	6.80 ± 8.53			
L4sp	0.32 ± 0.13	7.40 ± 10.81	L4	1.16 ± 1.58	1.21 ± 1.72
L4ss	0.52 ± 0.22	5.08 ± 6.05			
L5st	1.10 ± 0.43	0.97 ± 3.60	L5st	1.64 ± 1.26	2.75 ± 3.59
L5tt	3.53 ± 1.59	6.69 ± 9.19	L5tt	3.77 ± 3.25	3.99 ± 4.04
L6cc	0.87 ± 0.35	7.69 ± 6.67	L6cc	0.38 ± 0.19	1.66 ± 3.25
L6ct	0.08 ± 0.08	2.36 ± 5.39	L6ct	1.08 ± 1.91	0.78 ± 1.36

estimated distributions of VPM synapses were based on structural overlap between dendrites and axons.

3D Structure of Reconstructed Dendrite Morphologies in a Barrel Column

As far as extrapolation is concerned, we argue that the present dendrite morphologies can be regarded as representative samples that capture the anatomical variability of excitatory neurons within the vibrissal cortex (but see next section). Cortical neurons were usually searched for by monitoring resistance increase during current pulse application and at random cortical depths (Bruno and Sakmann 2006; de Kock et al. 2007). This yielded a sample that was largely unbiased with regard to the activity or location of a cell. Furthermore, we reconstructed the complete 3D morphologies of these in vivo-labeled neurons and registered all tracings with respect to 3D anatomical landmarks. Registration proved to be crucial to objectively classify morphological cell types, since it minimized the variability introduced by cutting the brain into slices and shrinkage during tissue fixation. In consequence, the anatomical parameters reported here were less affected by methodological artifacts (e.g., biased sampling, variability between preparations, cutting off dendrites). This may explain deviations from previous reports of dendrite morphologies. For example, the average dendrite length of a cell type was usually around ~30–50% longer when compared with in vitro studies (e.g., L2 [8578 µm vs. 4309 µm {Meyer, Wimmer, Hemberger, et al. 2010}], L4py [7492 µm vs. 2813 µm {Staiger et al. 2004}], and L6 neurons [5861 and 5899 µm vs. 3916 and 3868 µm for L6cc and L6ct pyramids, respectively {Kumar and Ohana 2008)}).

Finally, registration and objective classification of this unbiased sample of soma–dendrite morphologies allowed determining the vertical extent of somata of the 9 cell types. This revealed that cell type distributions do not necessarily match independently determined layer borders, which can be defined by various cytoarchitectonic criteria (e.g., soma density [Meyer, Wimmer, Oberlaender, et al. 2010]). Consequently, somata of multiple cell types may intermingle within and across cytoarchitectonically defined layers. Thus, the cell type–specific vertical boundaries and respective overlap ratios allowed for a more precise estimate of the number of neurons per cell type, when compared with previous studies that used cytoarchitectonic layers (Meyer, Wimmer, Oberlaender, et al. 2010).

Furthermore, the soma distribution and column dimensions in the present study reflected a stereotypic column, using average values. These values may deviate between individual columns and would thus affect the numbers of neurons per cell type (Supplementary Fig. S2*B*).

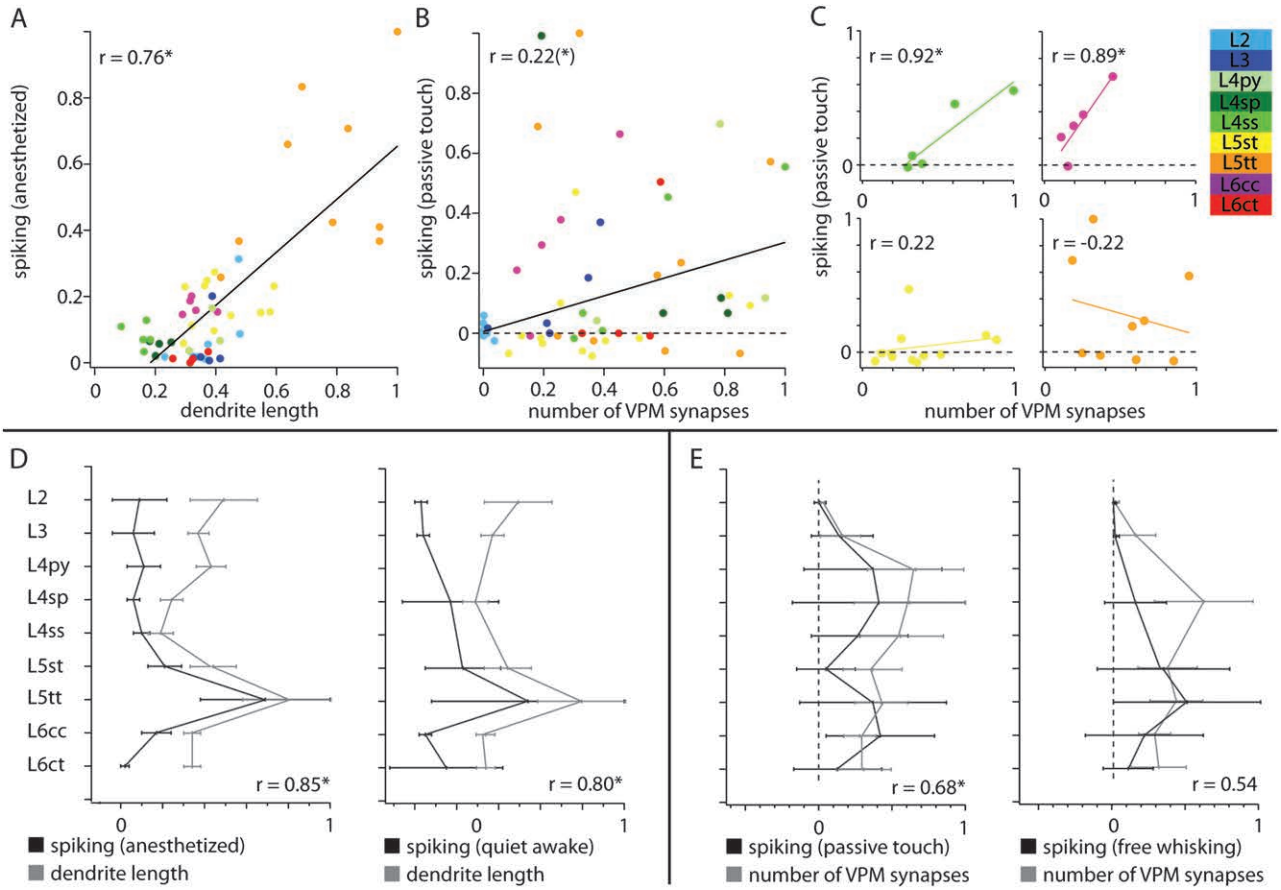

Figure 9. Cell type–specific structure–function relationships during different behavioral states. (*A*) Significant correlation between cell type–specific dendrite length and spontaneous spiking in the anesthetized state at single neuron level. (*B*) The cell type–specific evoked spiking (0–50 ms after passive touch) displays significant correlations with the number of VPM synapses at single neuron level. (*C*) Evoked spiking after passive touch displays high correlations for some cell types (e.g., L4ss and L6cc). Spiking in the remaining cell types is uncorrelated to the number of VPM synapses (e.g., L5st and L5tt). (*D*) Left panel: Significant (Bonferroni corrected) correlation between average cell type–specific dendrite length and average spontaneous spiking. Right panel: Significant correlation between average spontaneous spiking in awake animals and average dendrite length. (*E*) Left panel: The average cell type–specific evoked spiking (0–50 ms after passive touch) displays significant correlations with the average number of VPM synapses. Right panel: No significant correlation exists between the average numbers of VPM synapses and average spiking during free-whisking. All values in panels *D* and *E* are normalized to maximal mean + SD.

Excitatory Cell Types in a Barrel Column

As far as classification of cell types is concerned, we argue that the performed cluster analysis identified all dendritic cell types present in our sample. However, while we are confident that our sample of reconstructed morphologies comprises all excitatory dendritic cell types in L2/3 (Meyer, Wimmer, Hemberger, et al. 2010), L4 (Staiger et al. 2004), and L5 (Wise and Jones 1977), we did not observe some of the previously reported dendritic cell types in L6. For example, our sample did not comprise inverted pyramids and spiny bipolar cells (Zhang and Deschenes 1997). Furthermore, the limited sample size of L6cc cells did not allow for an unambiguous classification into further subtypes, as was suggested previously (Kumar and Ohana 2008). There, L6cc cells that displayed a decreasing length and number of apical oblique branches with increasing distance to the soma were distinguished from cells that displayed long oblique branches all along the apical dendrite. Finally, most of our reconstructed L6 neurons (L6cc and L6ct) were presumably located in cytoarchitectonic layer 6a (Fig. 2), which explains why we did not recover the large variety of dendrite morphologies reported for excitatory neurons in deep L6 (e.g., Chen et al. 2009).

In consequence, our estimated numbers of L6cc and L6ct pyramids per barrel column are likely an overestimate. However, slightly lower numbers of neurons per cell type would not affect the estimated vertical extents and dendrite innervation volumes of the 2 cell types in L6. More importantly, due to the sparse innervation of deep L6a and L6b by VPM axons, the estimated numbers and subcellular distributions of VPM synapses would also remain unchanged if the model column would be expanded by the missing cell types in L6.

In addition to classify morphological cell types by soma–dendrite features, subclasses of dendritic cell types may be identified by different axonal projection patterns. Distinct subcortical targets, for example among L5tt (corticothalamic vs. corticotrigeminal) and L5st (corticostriatal vs. callosal) neurons, have been reported previously (Hattox and Nelson 2007). These subtypes also varied in some of their dendritic and functional properties.

It remains to be investigated, if subtypes that are defined by different subcortical targets also display distinct intracortical axon projection patterns. In case of L5tt and L5st neurons, we previously reported the intracortical axon morphology of in vivo-labeled cells (Boudewijns et al. 2011; Oberlaender et al. 2011). There, we found that the intracortical axonal arbors were

significantly different (i.e., total length and target regions) between L5st and L5tt neurons. However, we did not study axonal specificity that would allow for a further subclassification of a respective dendritic cell type in layer 5.

Furthermore, it remains to be investigated if subtypes that are defined by distinct subcortical and/or intracortical targets are also located at different cortical depths. For example, L5st cells that project exclusively to the striatum are primarily found within cytoarchitectonic L5A (Hattox and Nelson 2007). In contrast, L5st cells that display collaterals to the striatum but project farther to the brain stem and spinal cord are primarily located in deeper regions of L5 (Hattox and Nelson 2007). We also found that slender-tufted pyramids are located in cytoarchitectonic layers L5A and B. However, we did not observe any obvious differences in dendrite morphology, VPM innervation, or spiking activity that would allow defining additional subtypes in L5.

In summary, by sampling only ~1% of all excitatory neurons within a barrel column, we cannot exclude the possibility that more than 9 excitatory dendritic cell types, or additional axonal subtypes (that may be revealed by future studies of reconstructing axons and dendrites of individual cells recorded in vivo), are present within a barrel column. However, identification of additional cell (sub) types would only affect the number of neurons per cell type estimated here. Thus, we provide an upper limit of neurons per cell type. Most importantly, the cell type–specific dendrite parameters, VPM innervation and spiking properties, reported here, would remain largely unchanged.

3D Structure of Reconstructed Thalamocortical Circuits in a Barrel Column

As far as axon–dendrite overlap is concerned (commonly referred to as Peter's rule [White 1979]), we argue that the approach used here yields valid first-order estimates of cell type–specific synaptic innervation because the 3D structure and distribution of somata, dendrites, and axons within the circuit model resemble the average structure of the real anatomical circuit. However, the validity of predicting synaptic connectivity by axon–dendrite overlap is arguably a matter of scale. It has been demonstrated that in general proximity of axons and dendrites does not predict synaptic connectivity at the (sub-) micrometer scale (e.g., Mishchenko et al. 2010; da Costa and Martin 2011). Furthermore, identification of higher order connectivity patterns or clustering of synaptic inputs on specific neurons or dendrite compartments may only be revealed by circuit reconstructions at the electron microscopy level (Bock et al. 2011; Briggman et al. 2011). Consequently, our estimates of synaptic connectivity are not based on geometrical proximity (i.e., touch) of axons and dendrites, as has been suggested previously (Kozloski et al. 2008).

Instead, overlap-based approaches at larger scales (e.g., 50 μm) yielded valid order of magnitude estimates of synaptic innervation for excitatory neurons (Lubke et al. 2003; Binzegger et al. 2004; Meyer, Wimmer, Hemberger, et al. 2010). Thus, we derived anatomical connectivity by determining realistic numbers of presynaptic axons-boutons and postsynaptic dendrites–spines and estimated innervation probabilities with 50-μm precision. While this approach neglects the possibility of axo-axonic connections (known to exist for GABAergic interneurons (e.g., Gonchar et al. 2002), our method represents the only feasible way to date for estimating excitatory connectivity at the scale of a cortical column and provides initial quantitative bounds for future studies of thalamocortical wiring at subcellular, cellular, and cell-type levels.

At the cell-type level, bulk labeling of VPM boutons in combination with in vitro-labeled dendrite morphologies was used previously to estimate the number and 1D innervation profile of VPM synapses for L2, L3, L4ss/sp, L5st/tt, and L6 neurons. Here, the superposition of individual VPM neurons resembled the innervation pattern obtained by bulk labeling (Meyer, Wimmer, Hemberger, et al. 2010). Furthermore, the previously estimated VPM bouton density in L4 and the rank order of VPM innervation of excitatory cell types was in good agreement to the bulk labeling data (Meyer, Wimmer, Hemberger, et al. 2010). At the cellular level, confocal imaging and serial electron microscopy studies estimated the number of anatomical contacts between single L4 neurons and the thalamus to be ~200 (da Costa and Martin 2011). Furthermore, paired in vivo recordings of VPM and L4ss neurons estimated an upper bound of ~600 synaptic release sites (Bruno and Sakmann 2006). This range was also in good agreement with our estimates for this connection type. Finally, at the subcellular level, innervation patterns obtained by channelrhodopsin-based synapse mapping, in vitro, between VPM and L3, L5st and L5tt neurons (Petreanu et al. 2009) resembled some of the maps obtained here.

In summary, the reconstruction of 3D anatomically realistic circuits reproduced the average connectivity results from the few studies that investigated thalamocortical innervation quantitatively (Bruno and Sakmann 2006; Petreanu et al. 2009; Meyer, Wimmer, Hemberger, et al. 2010; da Costa and Martin 2011). In addition, our approach allowed investigating the influence of the 3D soma location, dendrite morphology, and 3D VPM innervation on the number and pattern of synaptic contacts for every individual excitatory neuron in a barrel column. We found that thalamocortical innervation by VPM is not homogeneous within the barrel column in that axon (bouton) densities strongly deviated along the vertical and tangential column axes. Thus, the 3D soma location and the 3D dendrite morphology critically influenced the number and subcellular innervation pattern of synapses estimated for any neuron, even within the ensemble of a cell type.

For example, the average VPM synapse distribution across all L3 pyramids was asymmetric, with most synapses located in the lower basal dendrites, as consistently obtained by channelrhodopsin-based synapse mapping (Petreanu et al. 2009). However, such average cell type–specific connectivity maps have to be interpreted with caution, since synaptic innervation of individual neurons may deviate from the cell-type average. Thus, general conclusions drawn from average maps, such that all L3 pyramids receive VPM input at their distal, lower basal dendrites, which gave rise to speculations of sequential activation of dendrite subcompartments by distal and proximal inputs (Petreanu et al. 2009), may not hold for individual L3 neurons.

A second reason to interpret average cell type–specific connectivity maps with caution arises from the decay of thalamocortical synapses toward the tangential column border. For example, L4ss neurons located at the BCC displayed more symmetric dendrite morphologies than cells at the column border. There, L4ss dendrites projected predominantly toward the barrel center. Additionally, VPM bouton density was highest at the barrel center and decreased toward the borders. Both effects influenced the number and distribution of synapses per L4ss neuron, resulting in lower

connectivity values at the column border. In contrast, the average connectivity map across all L4ss in a column was symmetric and thus concealed differences in location-specific subcellular innervation patterns.

In summary, the present reconstruction revealed that structural overlap between VPM axons and dendrites of excitatory neurons can account for cell type– and location-specific synaptic innervations patterns of individual neurons. These order of magnitude estimates of the 3D structure of thalamocortical circuits at subcellular, cellular, and circuit levels finally allow relating cell type– and location-specific anatomical parameters to functional quantities, such as subthreshold responses and spiking activity recorded in vivo.

3D Structure of Thalamocortical Innervation Determines Cell Type–Specific Receptive Fields in a Barrel Column

Measurements of the receptive fields (RFs) of anatomically identified cell types, as measured by PSP amplitudes (postsynaptic potentials evoked by passive touch, recorded at the soma of a cell that is located in the respective column) represent the integrated synaptic input to the dendrites, where amplitude and time course depend on the 3D innervations and dendrite morphology. The PSP onset latencies for the different cell types were reported previously: L2, 18.3 ± 14.8 ms (Brecht et al. 2003); L3, 9.9 ± 4 ms (Brecht et al. 2003); L4, 8.0 ± 1.4 ms (Brecht and Sakmann 2002a); L5st, 10.1 ± 0.5 ms (Manns et al. 2004); L5tt, 10.1 ± 0.5 ms (Manns et al. 2004); L6, 9.8 ± 0.8 ms (R.M.B. and B.S., unpublished data). Thus, all cell types (with the exception of L2 neurons) are activated with comparable latencies (8.0–10.1 ms). This narrow time window strongly indicates that all cell types (with the exception of L2 neurons that show almost no overlap with VPM axons) are activated initially by the same input volley, originating from VPM (Brecht and Sakmann 2002b; Bruno and Sakmann 2006). The onset of whisker-evoked PSPs in L2 neurons, ~8 ms after this initial VPM volley, likely reflects subsequent intracortical activation (e.g., by L4ss neurons [Feldmeyer et al. 2002]).

Furthermore, the PSP-RFs vary substantially in their width for different cell types and their shape changes with time after stimulus onset (e.g., Brecht et al. 2003). For example, in L4ss cells, passive touch evokes a PSP that remains largely restricted to the 3D VPM-L4ss innervation domain estimated here, while the later widening of excitation into neighboring columns likely reflects a combination of L4 axon collaterals and thalamic surround whisker RFs (Egger et al. 2008). Furthermore, in L5tt neurons, passive touch initially evokes a column-restricted excitation that rapidly spreads into surrounding septa and columns (Manns et al. 2004). This may be due to the wide tangential spread of L5tt dendrites and VPM projections in the infragranular layers (Supplementary Figs S4 and S5). Finally, The PSP-RF of L5st pyramids is weaker than in the other cell types and remains column restricted. This reflects the anatomical observation that VPM innervation of L5st pyramids is densest in the apical oblique dendrites and innervation in basal dendrites is sparse, when compared with other cell types. Thus, the early synaptic input is probably weak and attenuated.

In summary, the 3D reconstruction of VPM axon and dendrite innervation domains is likely to provide an anatomical basis for the time dependent early (8–40 ms after passive touch) shapes of PSP-RF of excitatory cell types in a column.

3D Structure of Thalamocortical Innervation Determines Cell Type–Specific Spiking in a Barrel Column

In comparison to PSP input, the correlation between VPM innervation domains and spiking output of a cell type was expected to be much less direct, since several unknown intermediate steps connect the somatic PSP to spike generation. Nevertheless, correlation between spiking activity of ensembles and their number of potential VPM synapses was surprisingly high, suggesting that the cell type–specific initial synaptic input from VPM may contribute to the obtained cell type–specific spiking responses. In consequence, the anatomically defined cell types may also reflect functional ensembles with respect to spontaneous and whisker-evoked spiking after passive touch (Supplementary Fig. S6).

The correlation between spiking after passive touch and the number of VPM contacts was particularly pronounced for L3, L4ss, and L6cc neurons, where the number of VPM contacts may allow predicting whisker-evoked spiking at the single neuron level. In contrast, the lack of correlation for L5st, L5tt, and L6ct neurons suggests additional intracortical and/or cellular mechanisms, which conceal the thalamocortical input. In case of the L5 neurons, a large fraction of our sample displayed no change in activity or even decreased spiking, when compared with spontaneous activity. This may be caused by strong inhibitory feedback within L5, as was recently suggested by high densities of inhibitory interneurons in this layer (Meyer et al. 2011). The lack of whisker-evoked activity of L6ct neurons may be partially reflected by their membrane properties (Kumar and Ohana 2008), but our data suggest an additional anatomical explanation. Unlike other cell types in a barrel column, L6ct neurons received most VPM input within their apical tufts. Thus, attenuation of the VPM input by the apical dendrite may also lower the spiking probability of L6ct neurons, when compared with L6cc cells, which receive most VPM input within their basal dendrites.

Finally, VPM innervation and spiking activity during free whisking were less correlated, when compared with spiking activity after passive touch. This is possibly due to alternative thalamocortical pathways being activated during whisker motion (i.e., POm [Yu et al. 2006; Meyer, Wimmer, Hemberger, et al. 2010]) and/or direct neuromodulation of local cortical circuits (Constantinople and Bruno 2011).

Excitatory Cell Types Do Not Respect Layer Borders in a Barrel Column

Interpretation of functional data is usually performed in a layer-specific manner (i.e., for L2/3, L4, L5A, L5B, and L6), assuming that layers also reflect cell types (de Kock and Sakmann 2009; O'Connor et al. 2010). Here, we showed that at least 2 excitatory cell types were found in each layer and that their somata intermingle within layers and at the borders between them. Thus, especially when intermingling cell types differ in their biophysical properties and their axonal projection patterns, functional implications from electrophysiological recordings alone may be misleading without concomitant anatomical classification of the cell recorded from, which is subsequently illustrated by 4 examples.

We found that excitatory neurons in supragranular L2/3 can be objectively divided into L2 and L3 pyramids. L2 neurons remained almost silent after passive touch, while L3 pyramids

displayed on average 10-fold higher spiking frequencies than L2 cells. Furthermore, active L3 neurons were located close to the L4 border, where innervation by VPM is highest, again suggesting that location-specific synaptic connectivity relates to whisker-evoked spiking in vivo.

L4 contains 3 cell types that display similar spontaneous and whisker-evoked spiking responses. Thus, only post hoc identifications allowed for assignment of cell types. Furthermore, connectivity between VPM and L4 decreased toward the tangential column borders. This may result in a decay of spiking activity in L4 neurons toward the column borders after passive touch, as was recently predicted by network simulations (Lang et al. 2011). Such radial dependence was indeed described previously for the major targets of L4 neurons (Feldmeyer et al. 2002) in a barrel column (i.e., pyramidal neurons in L2/3 [Kerr et al. 2007]).

The L5st and L5tt pyramids intermingle except for narrow zones underneath L4 and above L6. Classification into L5A and L5B neurons may thus yield misleading results. This is of particular relevance since L5st and L5tt neurons may be key cell types to encode whisker motion and touch, respectively (Boudewijns et al. 2011; Oberlaender et al. 2011).

Finally, we found that the majority of L6cc neurons in our sample were robustly activated after passive whisker touch, whereas most L6ct pyramids remained inactive (P = 0.07 at trend level). L6ct neurons remain also inactive during free whisking, suggesting that the associated corticothalamic pathway (Deschenes et al. 1998) may only become active after combined input from VPM and motor cortex (Lee et al. 2008) during tactile-driven behavior.

Conclusions

Reconstructing the 3D structure of thalamocortical circuits between VPM and excitatory neurons in a barrel column yielded 5 major insights. First, we demonstrated that reconstruction of complete 3D morphologies and registration to anatomical reference structures were imminent prerequisites to define objective criteria that discriminate between cell types. Second, somata and dendrites of the obtained cell types intermingled within and across cytoarchitectonic layers. Thus, the layer containing the soma of a recorded neuron is not uniquely predictive of neuron morphology, cell type, presynaptic innervation, and functional responses. Third, reconstructing average 3D thalamocortical circuits yielded first-order estimates for the numbers and 3D distributions of somata, dendrites, and VPM synapses for the excitatory neurons in a barrel column. Fourth, structural overlap predicted that the number and subcellular distribution of VPM synapses is cell type- and location-specific. In particular, the 3D location of the soma may crucially influence synaptic connectivity, even for neurons of the same cell type. Fifth, correlations between cell type– and location-specific anatomical and functional features showed that 1) spontaneous spiking is correlated to the total dendrite length, 2) whisker-evoked spiking, elicited by passive touch is correlated to synaptic innervation by VPM, but 3) spiking during whisker motion is not significantly correlated to VPM innervation.

In summary, to assess the contribution of different cell types during behavior, the cell recorded from has to be anatomically identified and registered to determine its 3D location within the circuit. Even neurons located at exactly the same depth, for example, L5st and L5tt pyramids, display different dendrite morphologies, presynaptic innervation patterns, axonal projections (Hattox and Nelson 2007) and may even mediate different behavioral states (Oberlaender et al. 2011). Furthermore, neurons of the same cell type (e.g., L3 or L4ss neurons) can have different location-specific innervation patterns that may result in different spiking activity in response to the same stimulus. Thus, only identification of the cell type and soma location by post hoc reconstruction or genetic labeling (Groh et al. 2010) will allow estimating realistic synaptic innervation patterns that will help interpreting functional data to gain insights into cellular and subcellular mechanisms that underlie whisker-mediated behaviors.

Funding

Max Planck Society (to M.O., C.d.K, H.M., V.D., M.H., B.S.); the Center for Neurogenomics and Cognitive Research at the VU University Amsterdam (to C.d.K.); NINDS R01 NS069679, the Klingenstein Fund, the Rita Allen Foundation (to R.M.B.), and NIGMS T32 GM07367-35 (to A.R.).

Notes

We thank Andrea Weber, Sebastiano Bellanca, Thomas Mock, Merle Kurz, and Thorben Kurz for dendrite reconstructions, Tatjana Kleele for axon reconstructions, Albert Berman for implementing the clustering pipeline and Alexander Borst and David Fitzpatrick for comments on the manuscript. Author Contributions: M.O. and B.S. conceived and designed the project. C.d.K. and R.M.B. labeled cortical cells and provided dendrite reconstructions. R.M.B. and A.R. labeled VPM axons. C.d.K. recorded cortical spiking activity. H.M. provided confocal imaging data of NeuN-stained somata. V.D. implemented the network assembly tool. M.H. developed the registration tool. M.O. performed reconstructions, registrations, classifications, soma counts and network assembly, developed the data analysis routines, performed data analysis, and wrote the manuscript. *Conflict of Interest* : None declared.

References

Ankerst M, Breunig M, Kriegel HP, Sander J. 1999. OPTICS: ordering points to identify the clustering structure. In: Delis A, Faloutsous C, Ghandeharizadeh S, editors. ACM SIGMOD'99 International Conference on Management of Data; Philadelphia. (PA): ACM Press. p. 49–60.

Binzegger T, Douglas RJ, Martin KA. 2004. A quantitative map of the circuit of cat primary visual cortex. J Neurosci. 24:8441–8453.

Bock DD, Lee WC, Kerlin AM, Andermann ML, Hood G, Wetzel AW, Yurgenson S, Soucy ER, Kim HS, Reid RC. 2011. Network anatomy and in vivo physiology of visual cortical neurons. Nature. 471:177–182.

Boudewijns ZS, Kleele T, Mansvelder HD, Sakmann B, de Kock CP, Oberlaender M. 2011. Semi-automated three-dimensional reconstructions of individual neurons reveal cell type-specific circuits in cortex. Commun Integr Biol. 4:486–488.

Brecht M, Roth A, Sakmann B. 2003. Dynamic receptive fields of reconstructed pyramidal cells in layers 3 and 2 of rat somatosensory barrel cortex. J Physiol. 553:243–265.

Brecht M, Sakmann B. 2002a. Dynamic representation of whisker deflection by synaptic potentials in spiny stellate and pyramidal cells in the barrels and septa of layer 4 rat somatosensory cortex. J Physiol. 543:49–70.

Brecht M, Sakmann B. 2002b. Whisker maps of neuronal subclasses of the rat ventral posterior medial thalamus, identified by whole-cell voltage recording and morphological reconstruction. J Physiol. 538:495–515.

Briggman KL, Helmstaedter M, Denk W. 2011. Wiring specificity in the direction-selectivity circuit of the retina. Nature. 471:183–188.

Bruno RM, Sakmann B. 2006. Cortex is driven by weak but synchronously active thalamocortical synapses. Science. 312:1622–1627.

Celikel T, Sakmann B. 2007. Sensory integration across space and in time for decision making in the somatosensory system of rodents. Proc Natl Acad Sci U S A. 104:1395–1400.

Chen CC, Abrams S, Pinhas A, Brumberg JC. 2009. Morphological heterogeneity of layer VI neurons in mouse barrel cortex. J Comp Neurol. 512:726–746.
Constantinople CM, Bruno RM. 2011. Effects and mechanisms of wakefulness on local cortical networks. Neuron. 69:1061–1068.
da Costa NM, Martin KA. 2011. How thalamus connects to spiny stellate cells in the cat's visual cortex. J Neurosci. 31:2925–2937.
de Kock CP, Bruno RM, Spors H, Sakmann B. 2007. Layer and cell type specific suprathreshold stimulus representation in primary somatosensory cortex. J Physiol. 581:139–154.
de Kock CP, Sakmann B. 2009. Spiking in primary somatosensory cortex during natural whisking in awake head-restrained rats is cell-type specific. Proc Natl Acad Sci U S A. 106:16446–16450.
De Paola V, Holtmaat A, Knott G, Song S, Wilbrecht L, Caroni P, Svoboda K. 2006. Cell type-specific structural plasticity of axonal branches and boutons in the adult neocortex. Neuron. 49:861–875.
Dercksen VJ, Oberlaender M, Sakmann B, Hege HC. 2012. Forthcoming. Interactive visualization—a key prerequisite for reconstruction of anatomically realistic neural networks. In: Linsen L, Hagen H, Hamann B, Hege HC, editors. Visualization in Medicine and Life Sciences II. Berlin (Germany): Springer-Verlag.
Dercksen VJ, Weber B, Guenther D, Oberlaender M, Prohaska S, Hege HC. 2009. Automatic alignment of stacks of filament data. In: Proceedings of the IEEE International Symposium on Biomedical Imaging: from Nano to Macro (ISBI); 2009 Jun 28–Jul 1; Boston, MA., New York: IEEE. p. 971–974.
Deschenes M, Veinante P, Zhang ZW. 1998. The organization of corticothalamic projections: reciprocity versus parity. Brain Res Brain Res Rev. 28:286–308.
Egger V, Nevian T, Bruno RM. 2008. Subcolumnar dendritic and axonal organization of spiny stellate and star pyramid neurons within a barrel in rat somatosensory cortex. Cereb Cortex. 18:876–889.
Feldmeyer D, Lubke J, Silver RA, Sakmann B. 2002. Synaptic connections between layer 4 spiny neurone-layer 2/3 pyramidal cell pairs in juvenile rat barrel cortex: physiology and anatomy of interlaminar signalling within a cortical column. J Physiol. 538:803–822.
Furuta T, Deschenes M, Kaneko T. 2011. Anisotropic distribution of thalamocortical boutons in barrels. J Neurosci. 31:6432–6439.
Furuta T, Kaneko T, Deschenes M. 2009. Septal neurons in barrel cortex derive their receptive field input from the lemniscal pathway. J Neurosci. 29:4089–4095.
Gonchar Y, Turney S, Price JL, Burkhalter A. 2002. Axo-axonic synapses formed by somatostatin-expressing GABAergic neurons in rat and monkey visual cortex. J Comp Neurol. 443:1–14.
Groh A, Meyer HS, Schmidt EF, Heintz N, Sakmann B, Krieger P. 2010. Cell-type specific properties of pyramidal neurons in neocortex underlying a layout that is modifiable depending on the cortical area. Cereb Cortex. 20:826–836.
Hattox AM, Nelson SB. 2007. Layer v neurons in mouse cortex projecting to different targets have distinct physiological properties. J Neurophysiol. 98:3330–3340.
Helmstaedter M, de Kock CP, Feldmeyer D, Bruno RM, Sakmann B. 2007. Reconstruction of an average cortical column in silico. Brain Res Rev. 55:193–203.
Horikawa K, Armstrong WE. 1988. A versatile means of intracellular labeling: injection of biocytin and its detection with avidin conjugates. J Neurosci Methods. 25:1–11.
Hubel DH, Wiesel TN. 1959. Receptive fields of single neurones in the cat's striate cortex. J Physiol. 148:574–591.
Hutson KA, Masterton RB. 1986. The sensory contribution of a single vibrissa's cortical barrel. J Neurophysiol. 56:1196–1223.
Kerr JN, de Kock CP, Greenberg DS, Bruno RM, Sakmann B, Helmchen F. 2007. Spatial organization of neuronal population responses in layer 2/3 of rat barrel cortex. J Neurosci. 27:13316–13328.
Kozloski J, Sfyrakis K, Hill S, Schurmann F, Peck C, Markram H. 2008. Identifying, tabulating, and analyzing contacts between branched neuron morphologies. IBM J Res Dev. 52:43–55.
Kumar P, Ohana O. 2008. Inter- and intralaminar subcircuits of excitatory and inhibitory neurons in layer 6a of the rat barrel cortex. J Neurophysiol. 100:1909–1922.
Land PW, Buffer SA, Jr., Yaskosky JD. 1995. Barreloids in adult rat thalamus: three-dimensional architecture and relationship to somatosensory cortical barrels. J Comp Neurol. 355:573–588.
Land PW, Erickson SL. 2005. Subbarrel domains in rat somatosensory (S1) cortex. J Comp Neurol. 490:414–426.
Lang S, Dercksen VJ, Sakmann B, Oberlaender M. 2011. Simulation of signal flow in 3D reconstructions of an anatomically realistic neural network in rat vibrissal cortex. Neural Netw. 24:998–1011.
Larkman A, Mason A. 1990. Correlations between morphology and electrophysiology of pyramidal neurons in slices of rat visual cortex. I. Establishment of cell classes. J Neurosci. 10:1407–1414.
Lee S, Carvell GE, Simons DJ. 2008. Motor modulation of afferent somatosensory circuits. Nat Neurosci. 11:1430–1438.
Lubke J, Feldmeyer D. 2007. Excitatory signal flow and connectivity in a cortical column: focus on barrel cortex. Brain Struct Funct. 212:3–17.
Lubke J, Roth A, Feldmeyer D, Sakmann B. 2003. Morphometric analysis of the columnar innervation domain of neurons connecting layer 4 and layer 2/3 of juvenile rat barrel cortex. Cereb Cortex. 13:1051–1063.
Manns ID, Sakmann B, Brecht M. 2004. Sub- and suprathreshold receptive field properties of pyramidal neurones in layers 5A and 5B of rat somatosensory barrel cortex. J Physiol. 556:601–622.
Margrie TW, Brecht M, Sakmann B. 2002. In vivo, low-resistance, whole-cell recordings from neurons in the anaesthetized and awake mammalian brain. Pflugers Arch. 444:491–498.
Markram H. 2006. The blue brain project. Nat Rev Neurosci. 7:153–160.
Meyer HS, Schwarz D, Wimmer VC, Schmitt AC, Kerr JN, Sakmann B, Helmstaedter M. 2011. Inhibitory interneurons in a cortical column form hot zones of inhibition in layers 2 and 5A. Proc Natl Acad Sci U S A. 108:16807–16812.
Meyer HS, Wimmer VC, Hemberger M, Bruno RM, de Kock CP, Frick A, Sakmann B, Helmstaedter M. 2010. Cell type-specific thalamic innervation in a column of rat vibrissal cortex. Cereb Cortex. 20:2287–2303.
Meyer HS, Wimmer VC, Oberlaender M, de Kock CP, Sakmann B, Helmstaedter M. 2010. Number and laminar distribution of neurons in a thalamocortical projection column of rat vibrissal cortex. Cereb Cortex. 20:2277–2286.
Mishchenko Y, Hu T, Spacek J, Mendenhall J, Harris KM, Chklovskii DB. 2010. Ultrastructural analysis of hippocampal neuropil from the connectomics perspective. Neuron. 67:1009–1020.
Mountcastle VB. 1957. Modality and topographic properties of single neurons of cat's somatic sensory cortex. J Neurophysiol. 20:408–434.
O'Connor DH, Peron SP, Huber D, Svoboda K. 2010. Neural activity in barrel cortex underlying vibrissa-based object localization in mice. Neuron. 67:1048–1061.
Oberlaender M. 2009. Three-dimensional reengineering of neuronal microcircuits. Combined faculties of the natural sciences and for mathematics. Heidelberg (Germany): University of Heidelberg. p. 145–150.
Oberlaender M, Boudewijns ZS, Kleele T, Mansvelder HD, Sakmann B, de Kock CP. 2011. Three-dimensional axon morphologies of individual layer 5 neurons indicate cell type-specific intracortical pathways for whisker motion and touch. Proc Natl Acad Sci U S A. 108:4188–4193.
Oberlaender M, Broser PJ, Sakmann B, Hippler S. 2009. Shack-Hartmann wave front measurements in cortical tissue for deconvolution of large three-dimensional mosaic transmitted light brightfield micrographs. J Microsc. 233:275–289.
Oberlaender M, Bruno RM, Sakmann B, Broser PJ. 2007. Transmitted light brightfield mosaic microscopy for three-dimensional tracing of single neuron morphology. J Biomed Opt. 12:064029.
Oberlaender M, Dercksen VJ, Egger R, Gensel M, Sakmann B, Hege HC. 2009. Automated three-dimensional detection and counting of neuron somata. J Neurosci Methods. 180:147–160.
Oberlaender M, Ramirez A, Bruno RM. submitted. Sensory experience restructures thalamocortical axons during adulthood.
Peters A. 1979. Thalamic input to the cerebral cortex. Trends Neurosci. 2:1183–1185.

Petreanu L, Mao T, Sternson SM, Svoboda K. 2009. The subcellular organization of neocortical excitatory connections. Nature. 457:1142–1145.
Pierret T, Lavallee P, Deschenes M. 2000. Parallel streams for the relay of vibrissal information through thalamic barreloids. J Neurosci. 20:7455–7462.
Pinault D. 1996. A novel single-cell staining procedure performed in vivo under electrophysiological control: morpho-functional features of juxtacellularly labeled thalamic cells and other central neurons with biocytin or neurobiotin. J Neurosci Methods. 65:113–136.
Romand S, Wang Y, Toledo-Rodriguez M, Markram H. 2011. Morphological development of thick-tufted layer v pyramidal cells in the rat somatosensory cortex. Front Neuroanat. 5:5.
Staiger JF, Flagmeyer I, Schubert D, Zilles K, Kotter R, Luhmann HJ. 2004. Functional diversity of layer IV spiny neurons in rat somatosensory cortex: quantitative morphology of electrophysiologically characterized and biocytin labeled cells. Cereb Cortex. 14:690–701.
Stalling D, Westerhoff M, Hege HC. 2005. Amira: a highly interactive system for visual data analysis. In: Hansen CD, Johnson CR, editors. The visualization handbook. Burlington (MA): Elsevier. p. 749–767.
Welker C. 1976. Receptive fields of barrels in the somatosensory neocortex of the rat. J Comp Neurol. 166:173–189.
White EL. 1979. Thalamocortical synaptic relations: a review with emphasis on the projections of specific thalamic nuclei to the primary sensory areas of the neocortex. Brain Res. 180:275–311.
Wickersham IR, Finke S, Conzelmann KK, Callaway EM. 2007. Retrograde neuronal tracing with a deletion-mutant rabies virus. Nat Methods. 4:47–49.
Wickersham IR, Lyon DC, Barnard RJ, Mori T, Finke S, Conzelmann KK, Young JA, Callaway EM. 2007. Monosynaptic restriction of transsynaptic tracing from single, genetically targeted neurons. Neuron. 53:639–647.
Wimmer VC, Bruno RM, de Kock CP, Kuner T, Sakmann B. 2010. Dimensions of a projection column and architecture of VPM and POm axons in rat vibrissal cortex. Cereb Cortex. 20:2265–2276.
Wise SP, Jones EG. 1977. Cells of origin and terminal distribution of descending projections of the rat somatic sensory cortex. J Comp Neurol. 175:129–157.
Wong-Riley M. 1979. Changes in the visual system of monocularly sutured or enucleated cats demonstrable with cytochrome oxidase histochemistry. Brain Res. 171:11–28.
Woolsey TA, Van der Loos H. 1970. The structural organization of layer IV in the somatosensory region (SI) of mouse cerebral cortex. The description of a cortical field composed of discrete cytoarchitectonic units. Brain Res. 17:205–242.
Yu C, Derdikman D, Haidarliu S, Ahissar E. 2006. Parallel thalamic pathways for whisking and touch signals in the rat. PLoS Biol. 4:e124.
Zhang ZW, Deschenes M. 1997. Intracortical axonal projections of lamina VI cells of the primary somatosensory cortex in the rat: a single-cell labeling study. J Neurosci. 17:6365–6379.